Chapter 5
RELAY OPERATIONAL ANALYSIS DURING FAULT CONDITIONS

The previous chapters discussed relay specific algorithms and associated characteristics in detail, providing necessary insight for respective operation and fault resistive coverage under different system conditions. This chapter focuses on actual events that occurred in the Eskom transmission system over a number of years. These faults were selected due to specific problems with over-tripping of these lines. Wrong relay operation occurred for faults on the next busbar, faults behind the relay position and resistive faults for which plausible explanations had to be found. All event recordings shown contain analogue raw data and binary traces.

5.1 Sources of maloperation

In the cases under discussion, the following causes were identified as possible reasons for the protection over-tripping/maloperation events.

- Protection settings
- Faulty protection relay
- Incorrect line parameters
- Current transformer measuring errors
- Voltage transformer measuring errors

Incorrectly calculated or incorrectly applied settings could easily result in relay maloperation, whilst faulty protection relays normally result in no operation or operation without any cause.

Line parameters used in protection relay settings were originally calculated using the TMLC software tool provided by Power Technologies Incorporated. The

PowerFactory software provided by DigSilent was also used, and both software packages provided the same results. The results obtained from software calculations can only be as accurate as the inputs parameters provided. The source of these input parameters is the Transmission System Information System (TxSIS). This database is in the process of continuous verification and errors are therefore possible. Clear distinction is however made between verified and unverified data obtained from TxSIS.

Incorrect current transformer ratios or severe measuring errors can result in over or underreaching of protection devices. Incorrect voltage transformer ratios used in the calculation of settings or incorrectly calibrated voltage transformers can have the same impact as current transformers. Protection relay settings were scrutinized for possible errors, but were found to be in correlation with manufacturer's specifications and guidelines. Voltage and current transformer ratios as well as line impedance data from the central database were verified. The protection was subsequently re-tested and secondary non-intrusive playback techniques were used in all cases to simulate the actual fault conditions. The same results were obtained, which necessitated further investigation.

Sections 5.2, 5.3, 5.4, 5.5, 5.6 and 5.7 describe six different system events, their respective investigations, findings and corrective actions taken. The changes implemented and the impact of these changes will be discussed in section 5.8.

5.2 Athene – Invubu faults analysis

5.2.1 Incident

A single-phase-to-earth fault occurred on the C-phase busbar at Invubu substation on the 16th of October 2001 at 11:54:27 pm. The 7SA513 impedance protection relay at Athene substation overreached resulting in an incorrect instantaneous zone 1 trip at the Athene end.

5.2.2 Investigation and findings

The actual fault event records together with digital event traces are graphically illustrated in Figure 5.1, Figure 5.2 and Figure 5.3. Figure 5.1 depicts the three-phase voltage traces prior, during and after the fault, while Figure 5.2 represents the current traces for the same period. The blue-phase shows a major reduction in voltage indicative of a low resistance fault not far from the position of measurement. The current traces are somewhat misleading as a distinct relationship can be observed between the blue-phase and neutral currents, which are in phase and of similar magnitude, indicating a phase-to-earth fault. A significant increase and severe distortion of the red and white-phase currents occurred. This line is short, only 21.85 km long, which will result in this type of voltage depression on the faulted phase for faults towards the end of the line or for resistive faults.

Telemetered information received at the National Control Centre also indicated a busbar fault condition at Invubu at the same time as this event. The busbar at Invubu has gas insulated switchgear where all three-phases occupy the same chamber. It was found that the blue-phase had faulted inside the chamber resulting in a busbar fault at Invubu substation. No other faults were found on the line itself, and no other incidents on surrounding high voltage equipment were recorded.

It was concluded that the busbar fault could only have been the cause of a gas leak in the specific chamber resulting in insulation breakdown. It was also concluded that this was the root cause for the Athene – Invubu feeder trip. The resultant arcing inside the combined three-phase chamber was then also determined to be the reason for the distortions recorded on the red and B-phase currents.

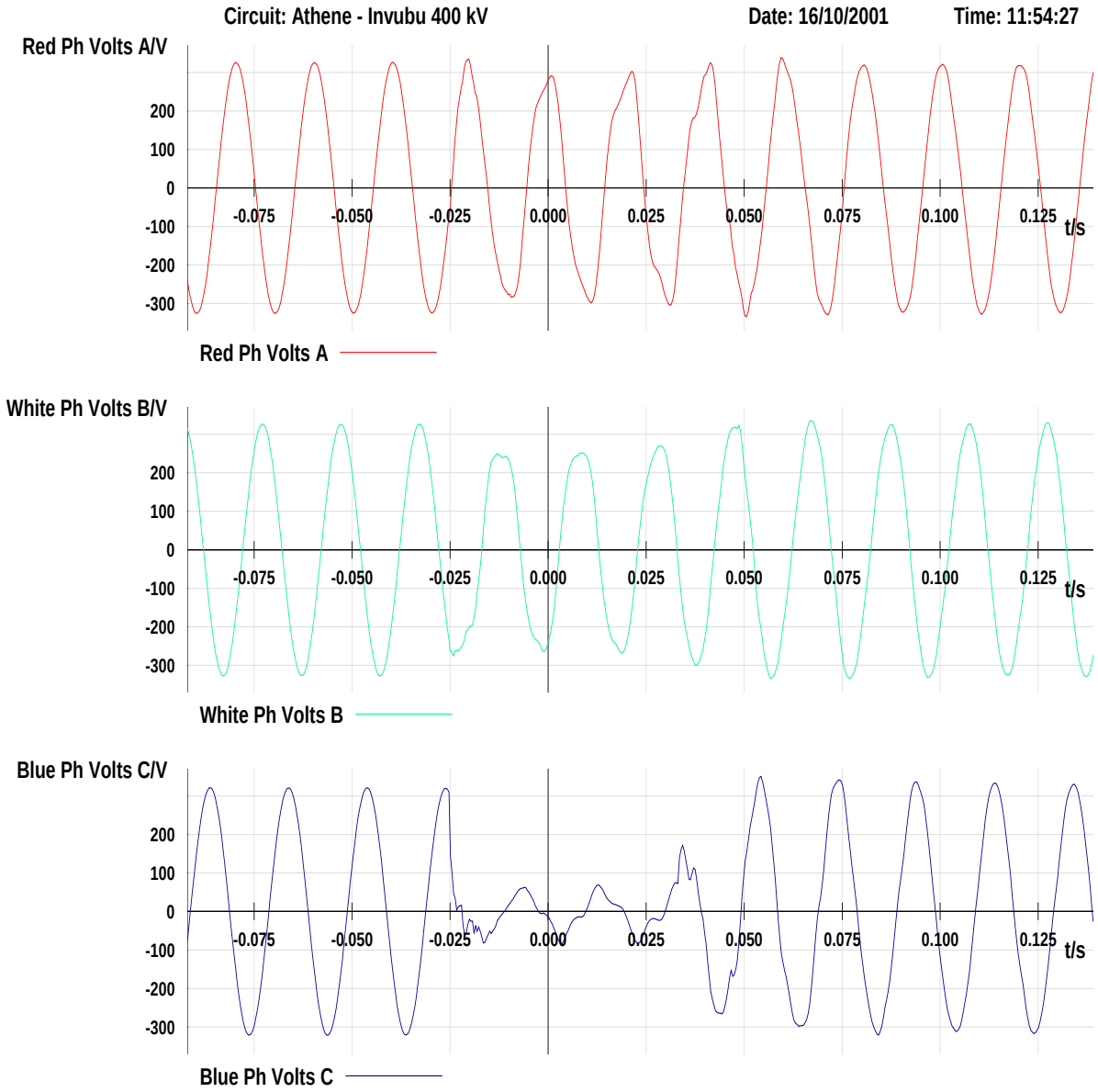

Figure 5.1: Voltage traces for Athene – Invubu incident

The digital traces revealed that the fault was originally detected as a single-phase-to-earth fault, which developed into a resistively coupled three-phase fault after approximately one-cycle, with an overall clearing time just exceeding 73.85 ms. The recording therefore shows that the Athene – Invubu feeder tripped within the instantaneous time frame confirming that the relay's zone 1 element overreached the total line length. Figure 5.4 shows the impedance locus at the time of fault superimposed on the relay characteristic in the positive sequence plane. The relay's reach clearly extended to the point of the fault. The actual reason for the relay's zone 1 overreach was not known.

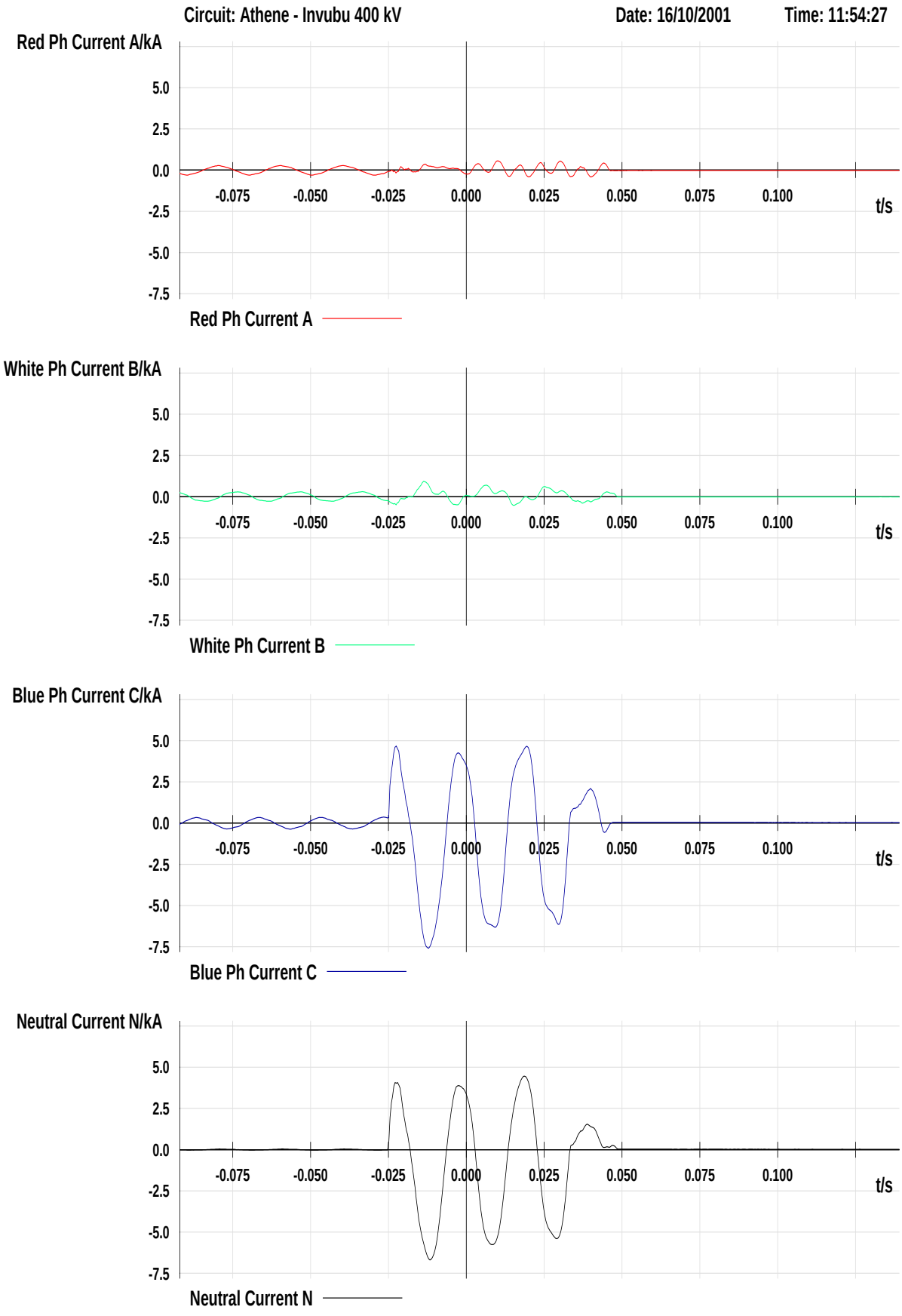

Figure 5.2: Current traces for Athene - Invubu incident

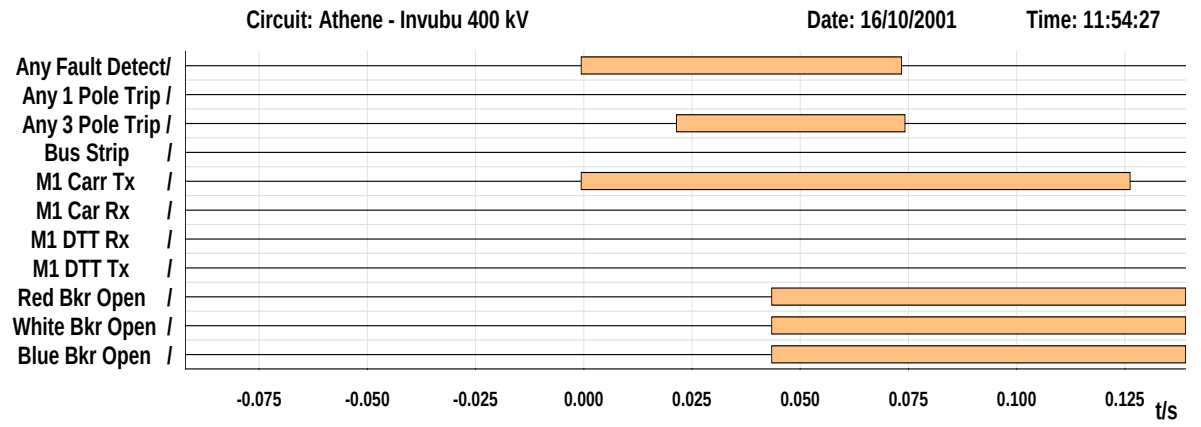

Figure 5.3: Digital traces for Athene - Invubu incident

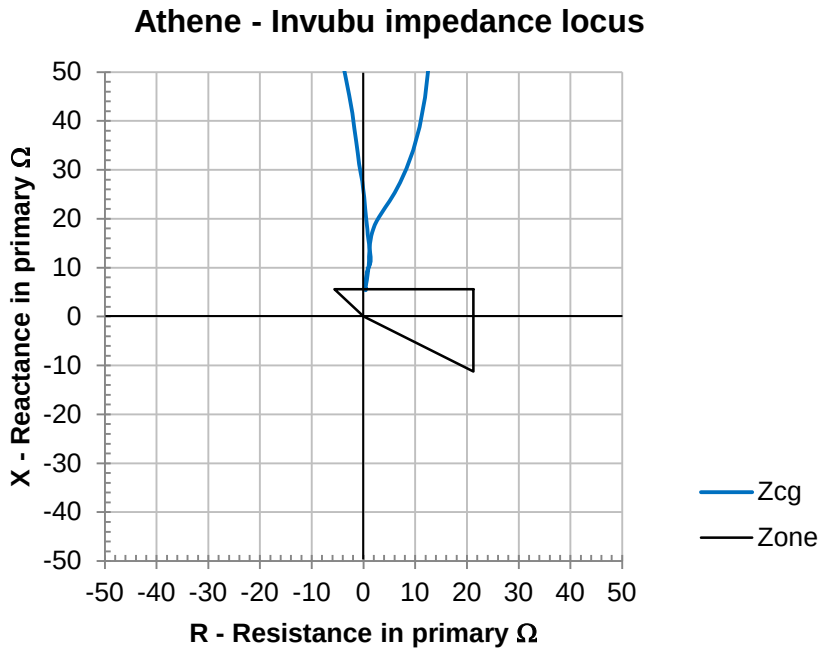

Figure 5.4: Athene - Invubu impedance locus at time of fault

Hillside Aluminium smelter is the biggest single electricity consumer connected to the Eskom transmission network. Due to the negative impact that system disturbances have on the very sensitive plant at the Hillside Aluminium smelter and other big industrial plants near Richards Bay, it was decided to actually measure the impedances of the overhead conductors. Details of the measurement techniques, test equipment, safety measures and actual measurement results are given in the following sub-section.

5.2.3 Overhead line impedance measurements

This section covers the theory involved in measurement of the overhead line impedance through primary injection methods. A comparison was made between the actual measurements and calculated values. The measurement is based on Ohm's law, which in complex format states that

$$Z\angle\phi = \frac{V\angle\phi_1}{I\angle\phi_2} \tag{5.1}$$

The importance of having accurate line impedance values inclusive of earth return impedance cannot be overstated. The correct operation of impedance type relays for all types of faults depends heavily on these values. Accurate values of positive (Z_1) and zero-sequence impedances (Z_0) are required for protection relay settings.

$$Z_1 = R_1 + jX_1 \tag{5.2}$$

$$Z_0 = R_0 + jX_0 \tag{5.3}$$

In order to measure transmission line impedance a number of factors need to be considered:

- Transmission line equivalent circuit;
- Test equipment needed and
- Safety precautions.

5.2.3.1 Transmission line equivalent circuit

It is important to ensure that the correct equivalent circuit for a transmission line is used, since an error would render any calculations made from measurements null and void. Figure 5.5 represents the transmission equivalent circuit used.

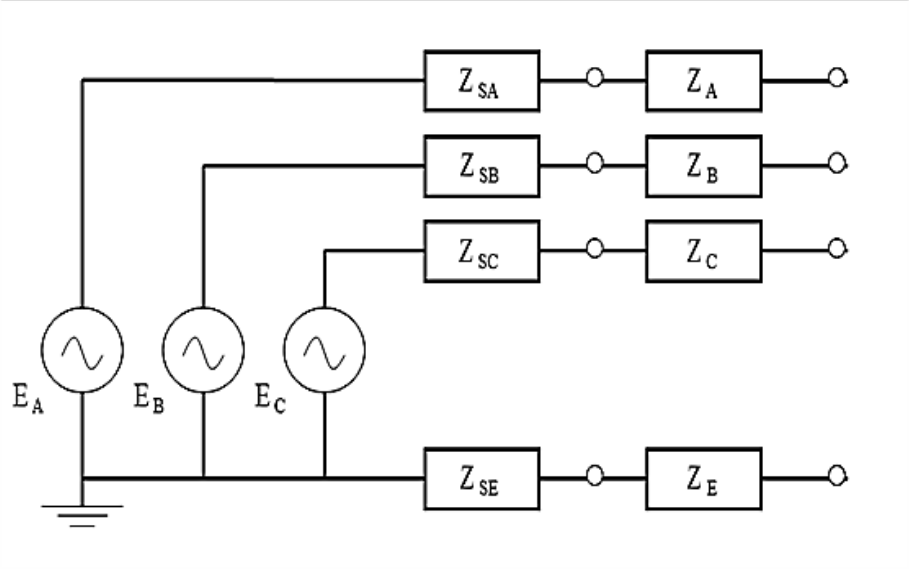

Figure 5.5: Transmission line equivalent circuit [14]

Currents were injected in the measuring loops A-B, B-C, C-A, A-N, B-N, C-N and A-B-C-N. Figure 5.6 illustrates the injection of current into the A-B phase loop. From these measurements the impedances Z_{A-B}, Z_{B-C}, Z_{C-A}, Z_{A-N}, Z_{B-N}, Z_{C-N} and Z_{ABC-N} could be determined.

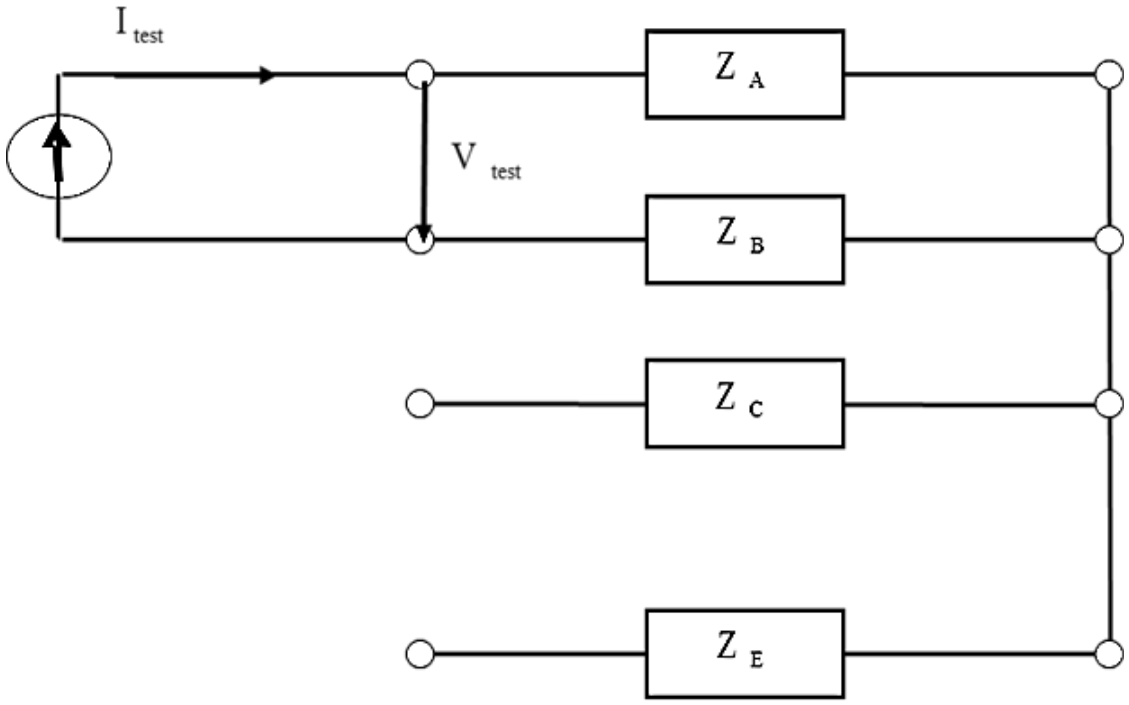

Figure 5.6: Injection test for A-B loop [14]

The following impedance relationships with reference to Figure 5.6 are valid [14]

Phase-to-phase impedance loops

$$Z_{A-B} = Z_A + Z_B \tag{5.4}$$

$$Z_{B-C} = Z_B + Z_C \tag{5.5}$$

$$Z_{C-A} = Z_C + Z_A \tag{5.6}$$

Phase-to-earth impedance loops

$$Z_{A-N} = Z_A + Z_E \tag{5.7}$$

$$Z_{B-N} = Z_B + Z_E \tag{5.8}$$

$$Z_{C-N} = Z_C + Z_E \tag{5.9}$$

Three-phase impedance loop

$$Z_{ABC-N} = \left[\frac{\left(\frac{Z_A Z_B}{Z_A + Z_B} \right) \cdot Z_C}{\left(\frac{Z_A Z_B}{Z_A + Z_B} \right) + Z_C} \right] + Z_E \tag{5.10}$$

Eq. (5.4) to Eq. (5.10) have four unknown variables from which, the different impedances Z_A, Z_B, Z_C and Z_E can be determined through mathematical manupulation.

$$Z_A = \left(Z_{A-B} + Z_{C-A} - Z_{B-C} \right) / 2 \tag{5.11}$$

$$Z_B = \left(Z_{B-C} + Z_{A-B} - Z_{C-A} \right) / 2 \tag{5.12}$$

$$Z_C = \left(Z_{C-A} + Z_{B-C} - Z_{A-B} \right) / 2 \tag{5.13}$$

From Eq. (5.11) to Eq. (5.13) and Eq. (5.10) the positive sequence impedance and the earth impedance in parallel with the earth-wire can be determined as shown in Eq. (5.14) and Eq. (5.15) [14].

Positive sequence impedance

$$Z_1 = Z_L = \frac{1}{3}\left(Z_A + Z_B + Z_C\right) \tag{5.14}$$

Earth impedance in parallel with earth-wire

$$Z_E = Z_{ABC-N} - \frac{Z_L}{3} \tag{5.15}$$

Alternatively, the earth impedance in parallel with the earth-wire can be calculated from Eq. (5.7) to Eq. (5.9) [14]

$$Z_E = \left[\left(Z_{A-N} - Z_A\right) + \left(Z_{B-N} - Z_B\right) + \left(Z_{C-N} - Z_C\right)\right] \tag{5.16}$$

From Eq. (5.14) and Eq. (5.16) the earth compensation factors and zero-sequence impedance of the line can be calculated as shown in Eq. (5.17) to Eq. (5.19).

$$k_L = \frac{Z_E}{Z_L} \tag{5.17}$$

and

$$\frac{Z_0}{Z_1} = 3k_L + 1 \tag{5.18}$$

therefore

$$Z_0 = (3k_L + 1) \cdot Z_1 \tag{5.19}$$

5.2.3.2 Test equipment

To facilitate accurate determination of a line's parameters with this method, it is imperative that accurate measurements of the injected current into the actual line as well as voltage are obtained. This is achieved with the use of a universal primary injection test set capable of injecting high currents at sufficient voltages. Accurate measurement of the amplitude and phase angle of the injected currents and voltages are required in order to give acceptable results.

For this test, equipment specifically developed for this purpose was used. The OMICRON CPC 100 [14] in conjunction with a CP CU20 coupling unit was used for these measurements. The CPC 100 universal primary injections test set is capable of injecting currents up to 800 A ac and 400 A dc with voltages up to 2000 V ac. It has the ability to accurately measure amplitude and phase angle for ac quantities as well as amplitude for dc voltages and currents. A schematic drawing of the test setup is given in Figure 5.7 [15]. The purpose of the CP CU20 unit is to provide galvanic isolation between the CPC100 test equipment, personnel and the high voltage overhead line to be tested by means of safety transformers for both the injected and measured signals. Pictures of these test sets are shown in Figure 5.8 and Figure 5.9. The CU20 transforms the output current from the CPC100, whilst a 500:100 V voltage transformer allows for safe voltage measurements. To eliminate test lead impedance a four-wire impedance measurement technique was used [15].

The horizontal distance parameters of both phase and earth conductors as well as the conductor diameter can be determined very accurately, usually to less than 1% error. It is however, impossible to determine the attachment height of the phase conductors and earth-wires above earth accurately. This is due to the varying height of towers along the length of a line, the earth profile changes as the line spans across valleys and sometimes canyons and the impact of vegetation growing to various heights under a line [15].

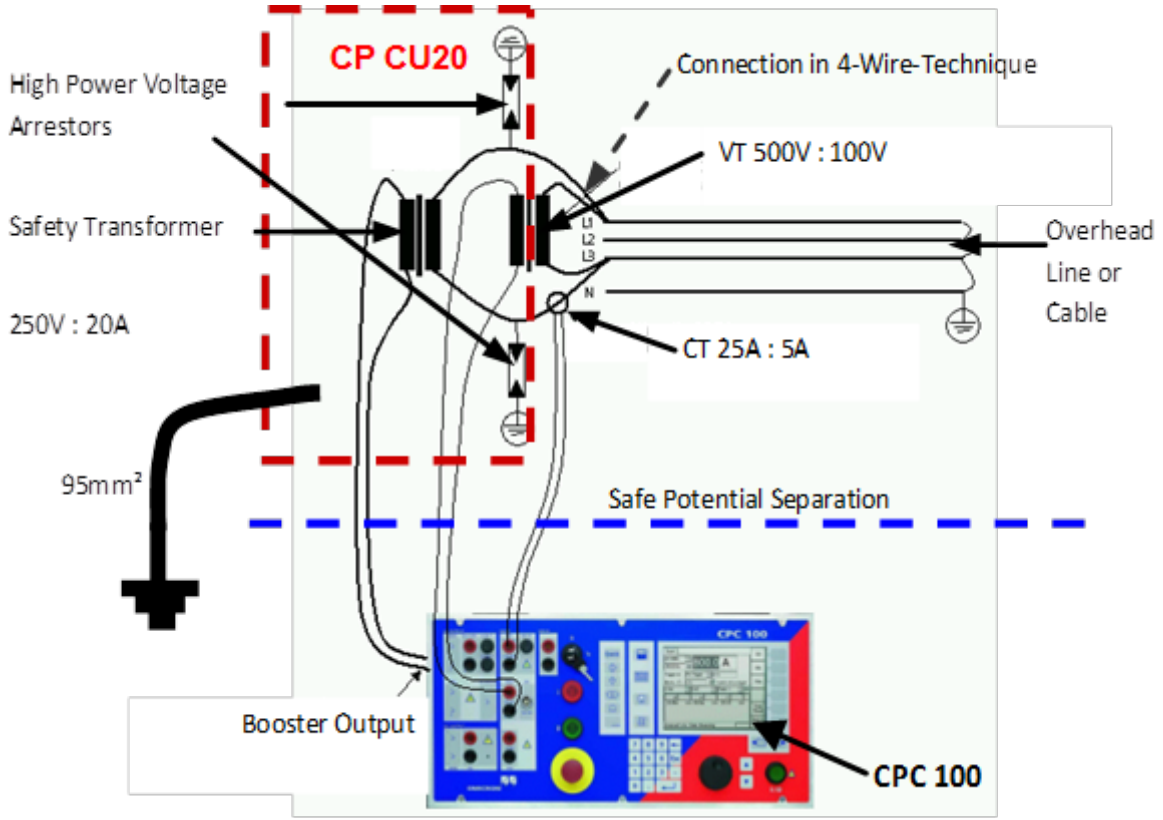

Figure 5.7: Schematic layout of line impedance test equipment [15]

Figure 5.8: CPCU20 unit [15]

Figure 5.9: CPC 100 primary injection test set [15]

During these tests it had been found that varying sag and/or varying conductor attachment height had negligible effect on the zero sequence impedance of a line. It had also been shown that earth resistivity had a similar effect on the zero sequence impedance [15].

5.2.3.3 Safety precautions

High voltage (HV) and extremely high voltage (EHV) overhead lines very often run together in the same servitude for long distances. It is therefore imperative that the inductive and capacitive coupling, which may exist between such lines be carefully analysed prior to performing any injection testing.

Capacitive coupling between a line running in parallel and the line under test and earth, could result in voltages up to 50% of nominal being induced, posing a very serious danger to the test equipment and human life. Inductive coupling between the parallel line and the line under test could cause high voltages to be induced in the line under test at the measuring end with the remote end earthed [15].

To mitigate the coupling effects it is essential that the following minimum precautions be taken [15]

- The remote end of line to be tested must be earthed via suitable earth switches and working earths for the full duration of these tests. Similar application to be used at the local end, with the exception that the working earths will also be used to inject test current.
- Prior to lifting of the local working earths, the induced capacitive current must be measured. An approximated capacitive voltage can then be calculated to determine the voltage that would be applied to the test equipment. The test equipment used was capable of safely handling induced capacitive voltages up to 500 V.
- Prior to disconnecting the working earth at the local end and connecting it to the test equipment, the local earth switch must be closed.
- For safety reasons nobody is allowed near any of the test leads once the earth switches has been opened to commence testing at the local end.

To eliminate interference at 50 Hz (the local system frequency, measurements are done at 30 Hz and 70 Hz. The results are then averaged to determine the equivalent result at 50 Hz [15].

5.2.3.4 Comparison of measured and calculated impedance

Factors that influence the accuracy of calculated overhead line impedances include [15]

- Earth resistivity changes with the type of soil and soil water content based on seasonal weather changes. Resistivity variations from as low as 30 Ωm to 1000 Ωm and higher are possible.
- Tower construction information in terms of height and conductor attachment heights must be correctly entered.
- Conductor and tower information entered.
- Earth-wire parameters. A good quality earth-wire nullifies the effect that earth resistivity has on the zero-sequence impedance of the line.
- Tower heights along the length of a line.
- dc-resistance of conductors.

The Athene-Invubu line has an overall length of 21.85 km and consists of two sections each with a different tower construction. Figure 5.10 gives an impression of the first tower on this line from Athene substation. Tower type 515 is used on the first 7.062 km and type 510 on the remaining 14.787 km, whilst the whole line is strung with twin dinosaur bundle conductor with 450 mm spacing. The earth-wire was given as stranded steel wire in the TxSIS database.

Figure 5.10: Tower 1 near Athene substation [15]

PowerFactory software was used to calculate the line impedance parameters. This software is capable of accepting different input methodologies. The tower geometry method allows for the entering of averaged conductor attachment heights and specific conductor detail was used. A value of 500 Ωm was used for the earth resistivity due to the time of year and the moisture content of the soil. With an averaged conductor sag of 30% of the average attachment height the positive and zero-sequence impedances were calculated and compared with those measured in Table 5.1 [15].

The line impedance was measured in June 2004 at 30 Hz, 50 Hz, 70 Hz, 90 Hz and 110 Hz to determine the linearity of the resistance and reactance measurements. The results of these tests are depicted in Figure 5.11. The deviation in resistance as well as reactance due to interference from the surrounding in service overhead lines is clearly visible for the 50 Hz test results. The corrected calculated values, as determined from the other frequencies are also indicated on the same graph [15].

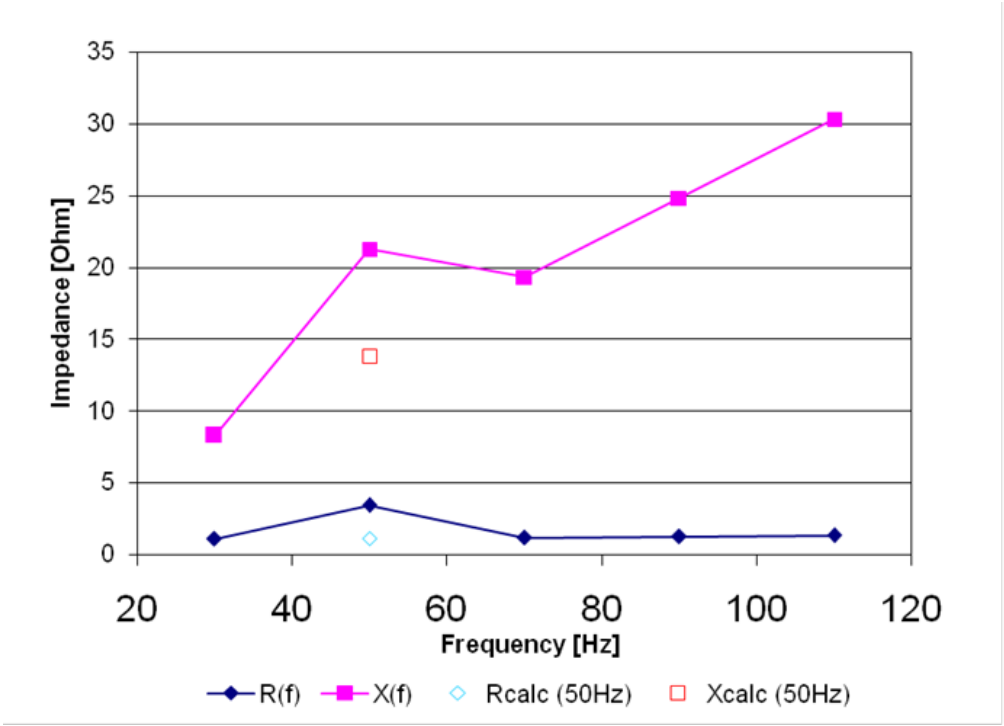

Figure 5.11: Frequency response of resistance and reactance [15]

Table 5.1: Impedance comparison for Athene - Invubu line

Calculated values	Measured values	Percentage deviation	
Z1 = 0.543 + j7.019	Z1 = 0.587 + j7.128	R1 = -8.1 %	X1 = -1.53 %
Zo = 6.702 + j23.825	Zo = 4.623 + j16.067	Ro = 31.02 %	Xo = 32.56 %

The percentage deviation calculated, using the calculated values as reference, illustrated a significant error in either the measurement or the calculated values for the zero sequence impedances. Due to the tower height as illustrated in Figure 5.10 the type and size of the earth conductor could not be established from ground level. On closer inspection it was found that Greased Horse and Greased Tiger earth-wire conductor was used on the two sections of line respectively. These earth-wires have significantly different impedances when compared with steel earth-wires and are therefore the root cause for the difference between the calculated values and those measured. The overhead lines database therefore did not reflect the actual as built earth conductor information. The calculations were re-done using the correct earth-wire parameters, which resulted in the values shown in Table 5.2.

Table 5.2: Corrected impedance values for Athene - Invubu line

Calculated values	Measured values	Percentage deviation	
Z1 = 0.540 + j6.770	Z1 = 0.587 + j7.128	R1 = -8.7 %	X1 = -5.29 %
Zo = 4.192 + j15.837	Zo = 4.623 + j16.067	Ro = -10.28 %	Xo = -1.45 %

The measured impedances compared favourably with those calculated by PowerFactory, with relatively small deviations of 8.7% for R_1, 5.29% for X_1, 10.28% for R_0 and 1.45% for X_0 between calculated and measured impedances. (A summary of line impedance test results are available in Appendix E.) Of interest is the fact that the positive sequence inductive reactance also changed with the new calculated values. In an attempt to determine where the differences, which still exist between the calculated and measured values, originate from an analysis on the impact of dc-resistance variations on the conductor impedance was performed by [15].

The result of this analysis is depicted by the curves shown in Figure 5.12 indicating the relationship between dc-resistance and zero-sequence impedance of a typical EHV line [7]. From Figure 5.12 it can be observed that for an earth-wire conductor dc-resistance of between 0.1 Ω/km and 10 Ω/km the zero-sequence resistance (R_0) and inductance (X_0) varies significantly. This is a very important observation, since typical values of dc-resistance for different types of conductors used fall in this range. It therefore follows that should an incorrect dc-resistance value for the earth-wire conductor be used to calculate a specific lines impedance values, a significant variation from the actual line zero sequence impedance could result.

Figure 5.12 shows that for specific values of dc-resistance, the zero sequence resistance actually decreases, whilst the zero sequence reactance increases rapidly. This phenomenon is therefore thought to be the reason for the differences that exist in the final result comparison.

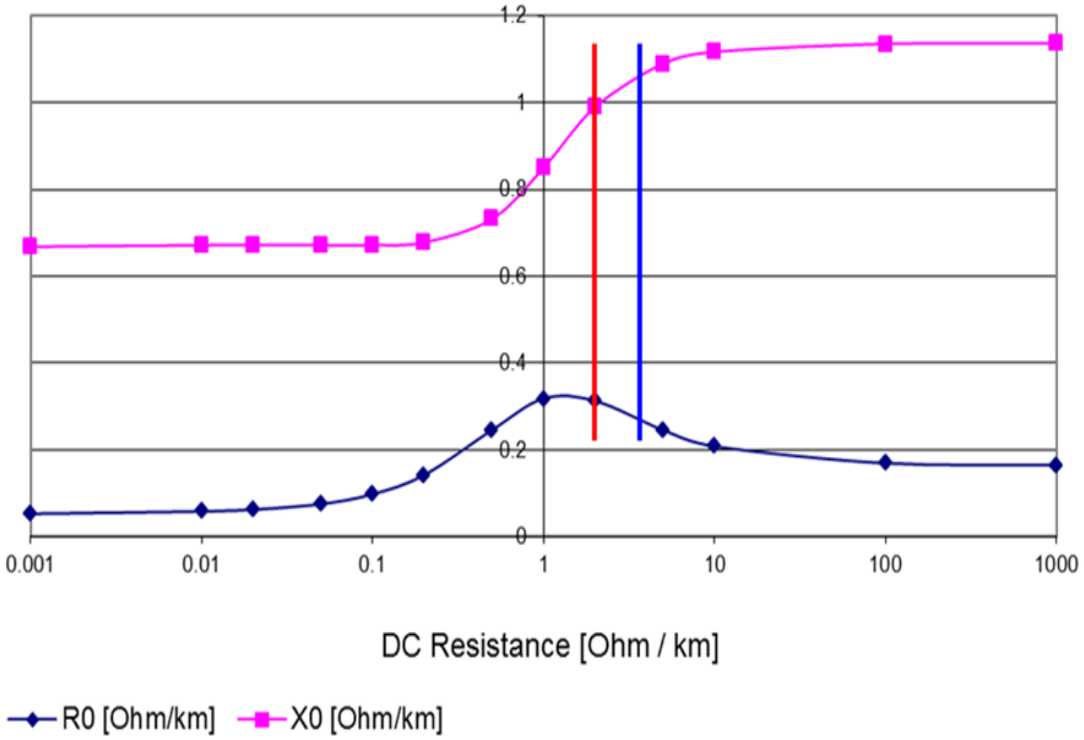

Figure 5.12: dc-resistance sensitivity analysis [7]

The conclusion was therefore that the protection settings had to be revised to suit the correct line parameters. In order to be consistent, it was however, decided to use the calculated values rather than the measured values. Changes to the protection settings will be discussed in section 5.8.

5.3 Hydra – Perseus fault analysis

5.3.1 Incident

An incident, which occurred on the 400 kV busbar at Perseus substation, nearly resulted in a major system incident when two 400 kV feeders linking generation in the North to generation in the South of South Africa, tripped in sympathy.

5.3.2 Investigation and findings

On the 5th of May 2005 at 15:29 a 400 kV B-phase current transformer on Perseus number 1 Static Var Compensator failed. The fault was cleared successfully by the Static Var Compensator protection, tripping the associated 400 kV breaker, effectively isolating the Static Var Compensator equipment, inclusive of harmonic

filters and capacitor banks from the system. The second Static Var Compensator remained in service. 1.5 s later an A-phase to B-phase busbar fault developed, most probably due to the amount of smoke released from the failed current transformer, and was cleared correctly by the bus zone protection.

The Hydra – Perseus and Leander – Perseus feeder protection overreached resulting in incorrect tripping and auto re-closing of these 400 kV feeders. This section will focus on the Hydra –Perseus line, which tripped on B-phase in zone 1 reach and re-closed. Hydra and Perseus substations form a very important link in the Eskom transmission power grid in that it interconnects the generation in the north to Koeberg in the south. Loss of this connection due to a system fault could result in severe system instability due to the imbalance created between power generated and demand. The interconnectivity between these two stations is shown in Figure 5.13.

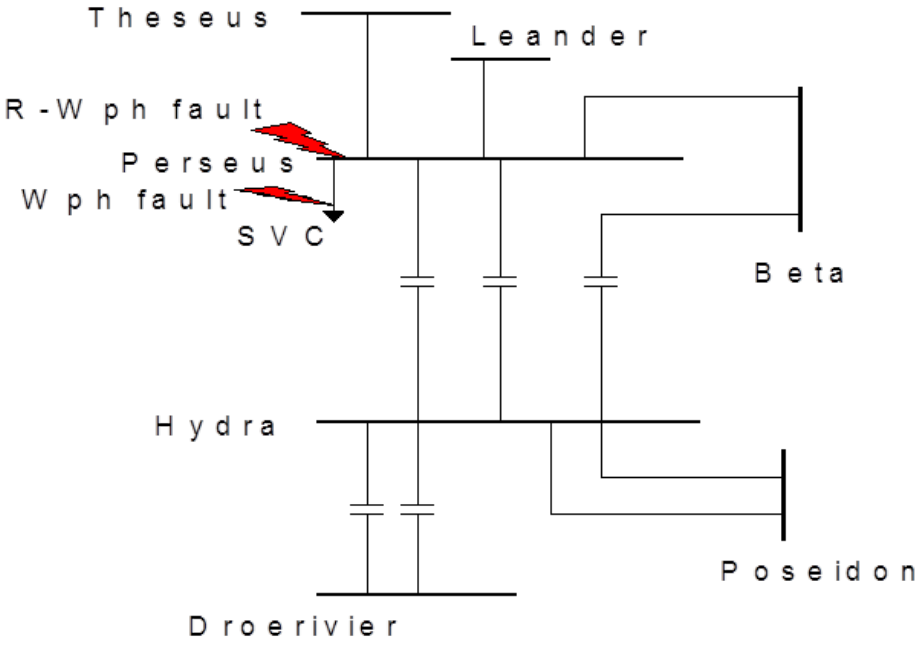

Figure 5.13: Network interconnectivity diagram

This 400 kV line, at 283.2 km, is one of the longest lines in the Eskom transmission system and has been series compensated at mid-point with a percentage compensation of 52.76% to improve power transfer capability. The actual fault recording as seen from Hydra substation is shown in Figure 5.14 and Figure 5.15, from which the impact on the system voltage can be observed. The initial B-phase-

to-earth fault caused by the failure of the 400 kV Static Var Compensator current transformer was cleared in 90.6 ms by its own protection. The voltage traces in Figure 5.14 shows two white-phase voltage dips, similar in magnitude. The Hydra – Perseus circuit did not trip for the first instance as is also indicated by the binary signals in Figure 5.16. The second fault, which was caused by the A-phase to B-phase busbar fault, was cleared in 68.23 ms. The protection on the Hydra – Perseus circuit incorrectly operated for the red-to-white-to-earth fault. From the binary traces in Figure 5.16, it can be seen that the B-phase current returns after approximately 1.25 s, whereas the normal dead time for a single-phase auto-re-closure is 1 s, showing an additional delay.

The binary traces shown in Figure 5.16 confirms the relay operation as discussed and also confirms that the fault had been behind the remote end (Perseus – Hydra) feeder protection.

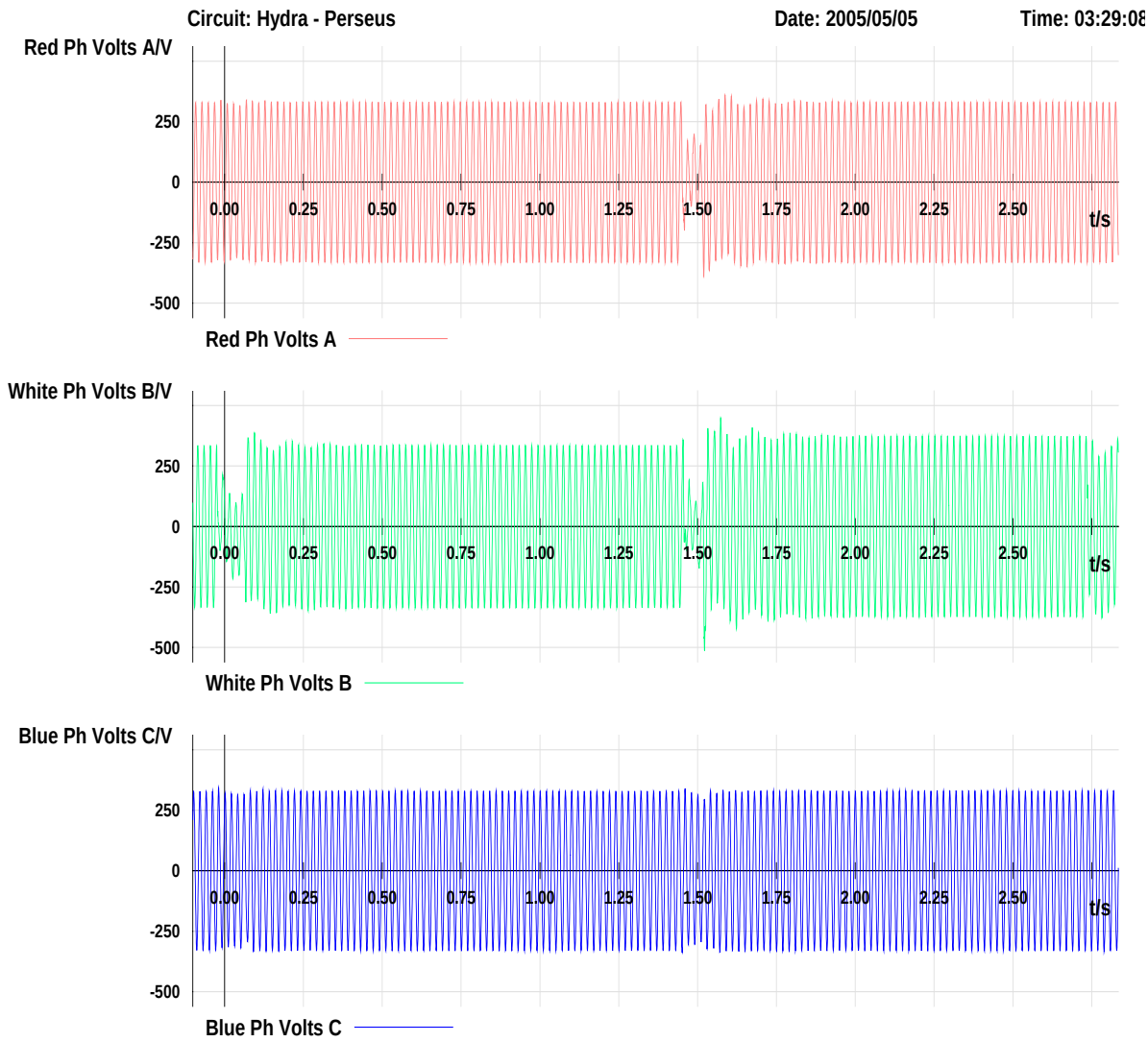

Figure 5.14: Voltage traces for Hydra - Perseus fault

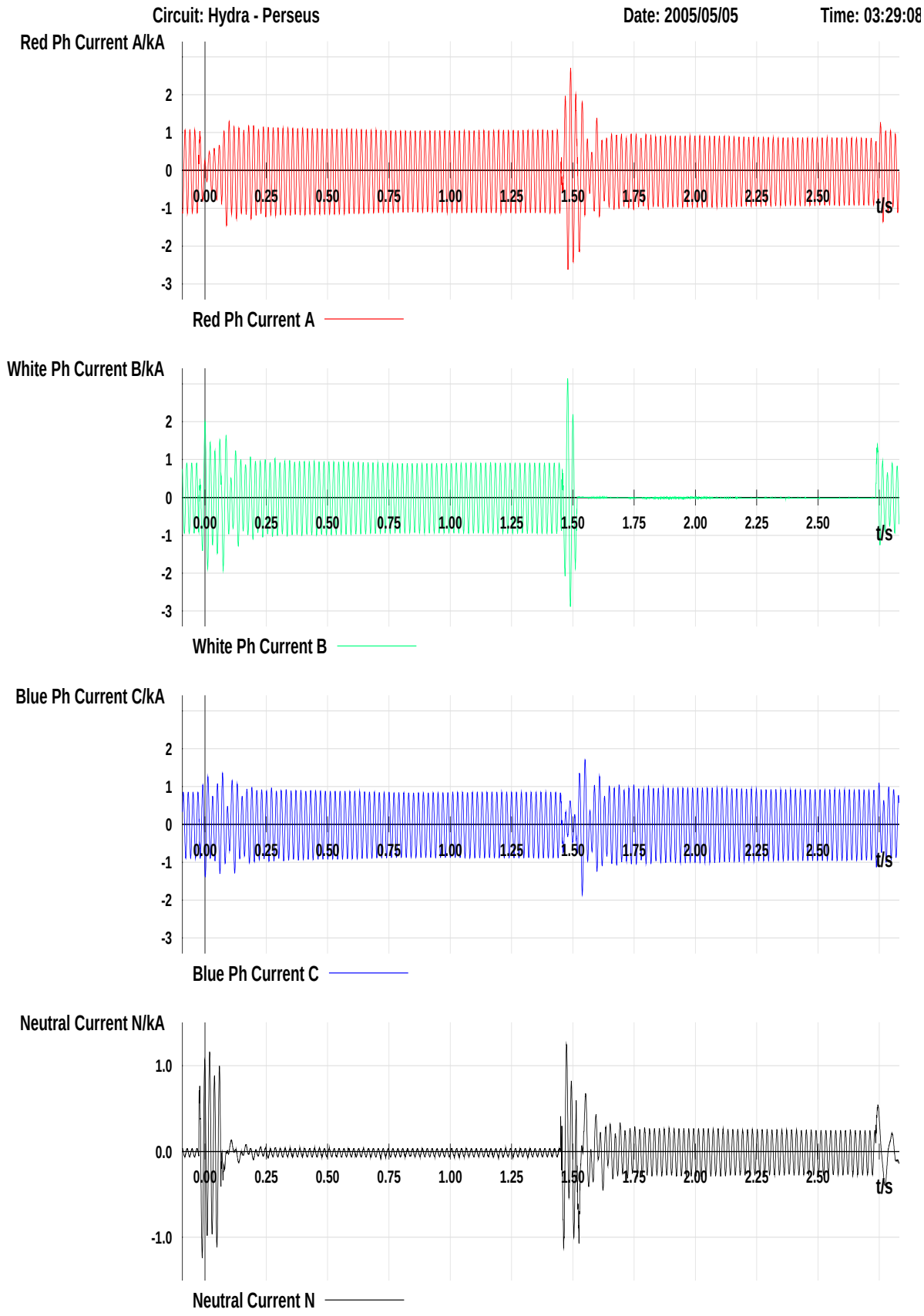

Figure 5.15: Current traces for Hydra - Perseus fault

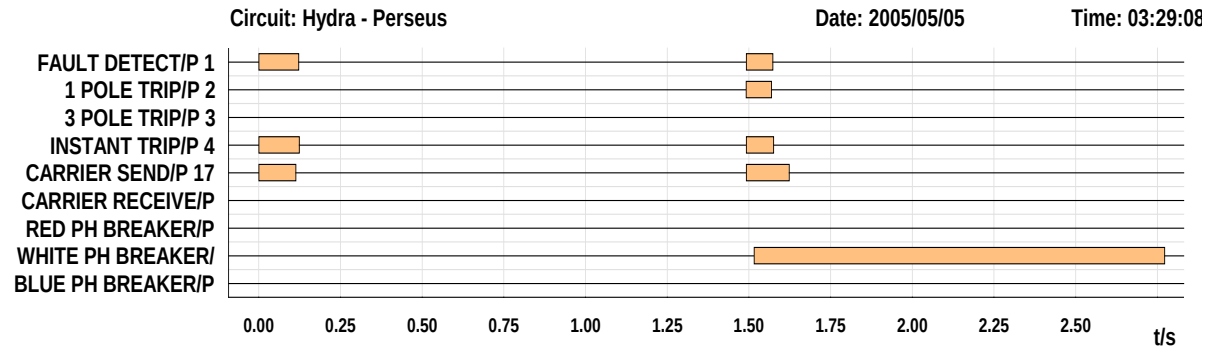

Figure 5.16: Binary signals for Hydra - Perseus fault

Enlarging the second fault portion of the voltage and current traces to enable greater observability results in the graphs shown in Figure 5.17 and Figure 5.18. From the voltage traces can be observed that some harmonic distortion was responsible for the non-sinusoidal waveform during the fault. The A-phase and B-phase current traces show a fair amount of harmonic distortion at fault inception and during the fault. Figure 5.19 graphically illustrates the impedance locus of the B-phase (Z_{bg}) at the time of fault. The extent of overreach for this fault on the Perseus busbar is shown in Figure 5.19.

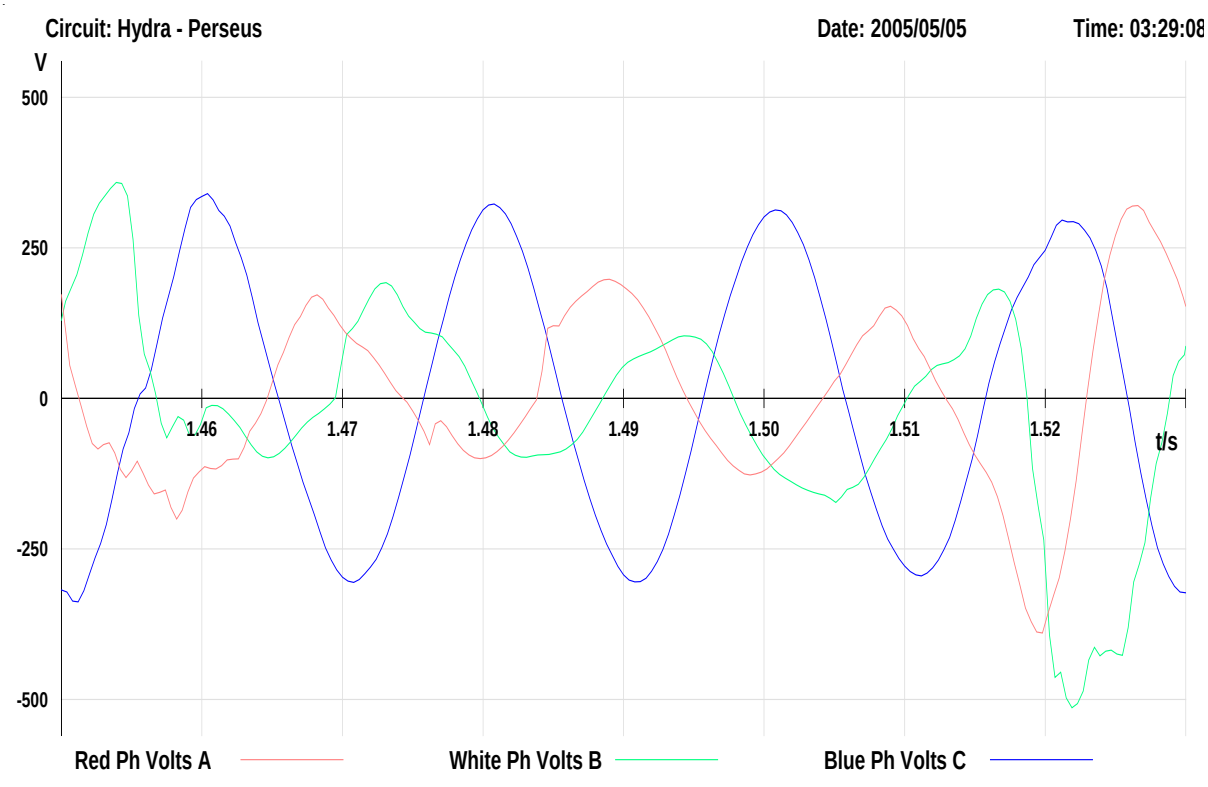

Figure 5.17: Enlarged voltage traces for Hydra - Perseus fault

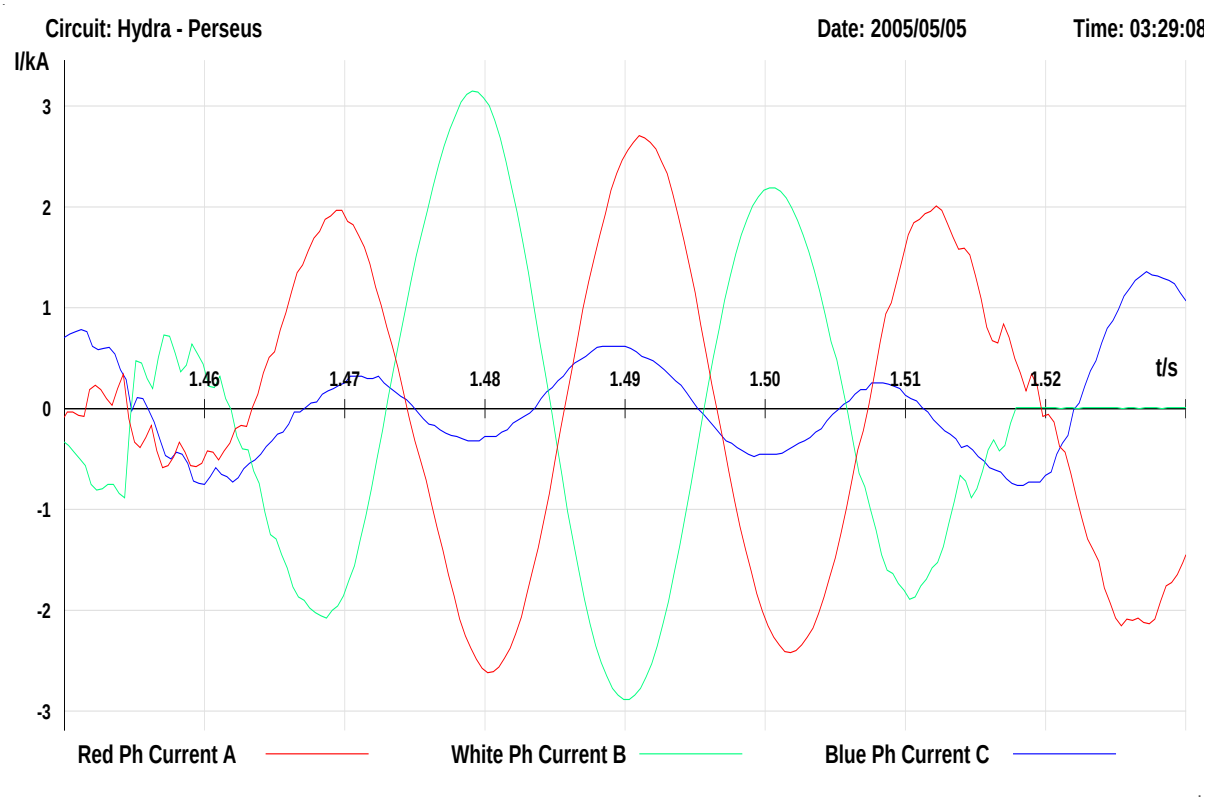

Figure 5.18: Enlarged current traces for Hydra - Perseus fault

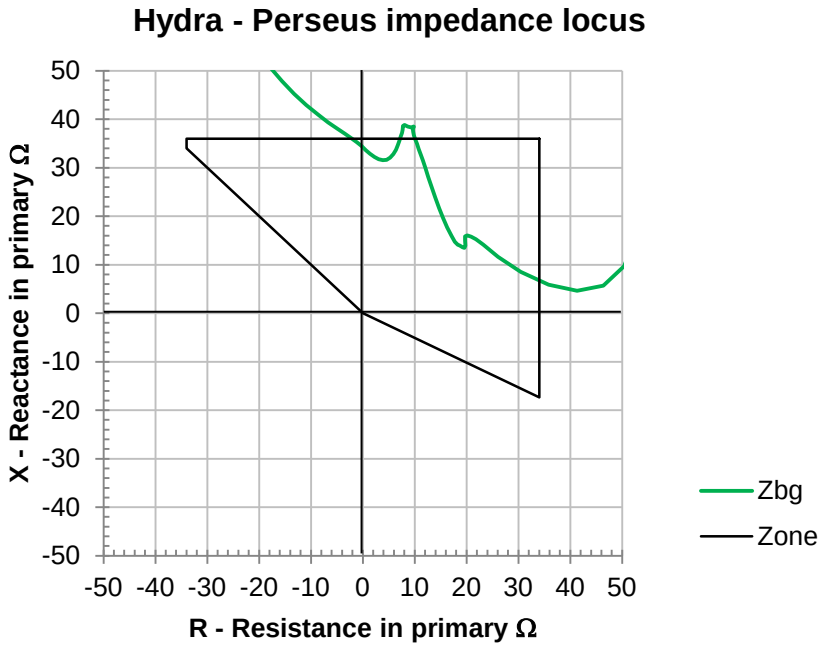

Figure 5.19: Hydra - Perseus impedance locus at the time of fault

In order to eliminate all possible errors, it was decided to have the line impedance measured. This was also done previously on the Athene - Invubu line with great success. It was possible that measuring the Hydra – Perseus line would show

similar results. Table 5.3 shows a comparison between the calculated values used in the setting calculation and the actual line impedance measured. The calculated values were used as reference.

Table 5.3: Impedance comparison for Hydra - Perseus line

Calculated values	Measured values	Percentage deviation	
Z1 = 7.616 + j90.064	Z1 = 7.653 + j95.120	R1 = -0.49 %	X1 = -5.61 %
Zo = 87.712 + j307.76	Zo = 95.181 + j292.871	Ro = -8.51 %	Xo = 4.84 %

This table also shows the calculated values for the positive, zero sequence resistance and the positive sequence reactance to be less than the actual measured values, whilst that for the zero sequence reactance is greater than measured. This phenomenon can be explained using the conductor dc-resistance phenomena discussed before (see Figure 5.12). Using the vertical red line on the graph as the measured impedance line with the vertical blue line as the calculated impedance, the same correlation was obtained. It therefore represents a difference in the actual dc-resistance of the earth-wire used to that used in the impedance calculation.

The differences obtained is however insignificant, since during protection relay setting calculations a 20% safety margin is used to cater for line impedance, current and voltage transformer inaccuracies. The calculated values are mostly smaller than actual, which further reduces the chances of relay overreach. Zone 1 reactive reach (X1) were set at 75% of the line inductive reactance minus the capacitor reactance. This is in line with the theory discussed in Chapter 3, Eq. (3.7) refers. The capacitor banks at Luckhoff use a spark gap and MOV (Metal Oxide Varistor) to protect against high overvoltages that would result during high fault currents. The additional transient compensation referred to by [6], see Eq. (3.8), required for MOV protection had not been used. Metal Oxide Varistors react based on the amount of current flowing through them, and as such changes the overall series capacitor impedance. The interaction between the MOVS and the system causes a varying harmonic frequency resonance, and it is because of this resonance that the additional transient compensation is required.

This transient compensation factor had been overlooked since no such requirement was given in the performance guarantee limit documentation of the 7SA513 relay [21]. The final impact of the revised settings based on the harmonic oscillations will be discussed in detail in section 5.8.

5.4 Georgedale – Klaarwater faults analysis

5.4.1 Incident

On the 18th of June 2002 at 08:34:15 an A-phase-to-earth fault occurred on an adjacent feeder to the Georgedale – Klaarwater 275 kV feeder. The Georgedale – Klaarwater feeder tripped in sympathy for this fault.

5.4.2 Investigation and findings

The protection on the adjacent feeder had correctly operated and cleared the fault in zone 1 time. For the Georgedale – Klaarwater feeder, this was a reverse fault and should not have had any impact on its protection. The voltage and current traces shown in Figure 5.20 and Figure 5.21 provided no additional information, except to confirm that the fault was in fact a reverse fault. This can be seen when evaluating the sudden change in the A-phase current loci, which changes from 6.7 ms (120°) ahead of the B-phase (C1 and C2 shown in dotted lines in Figure 5.23), at around 0.065 s before the point of trigger, to approximately 13.8 ms (248.4°) before when comparing the next zero-crossing (C1 and C2 shown in solid lines in Figure 5.23).

The change in direction of the A-phase current as well as the angular comparison with the B-phase is graphically illustrated in Figure 5.23 and Figure 5.24. Vertical markers C_1 and C_2 illustrate this phenomenon, which equates to an approximate 128.4° change in direction.

The binary signals shown in Figure 5.22 indicate that the feeder had in fact tripped three-phase. The breaker poles opened between 28 ms and 29.2 ms after receiving the carrier signal from the remote end. Under normal conditions the protection at the Georgedale end should have blocked any tripping from occurring due to the fact that

a permissive overreach tripping scheme is in use. Plotting the different impedance loci against the relay characteristic in the positive sequence plain revealed some interesting facts (see Figure 5.25).

Although the faulted A-phase-to-earth (Z_{ag}) impedance is correctly positioned in the third quadrant, the healthy C-phase-to-earh (Z_{cg}) is situated in the first and fourth quadrants and enters the relay zone 1 forward reaching characteristic. The result is that a A-phase-to-earth fault is detected in reverse whilst a C-phase-to-earth fault is also detected in the forward direction, resulting in wrong phase selection. Reception of the remote end carrier together with the red- and C-phase impedance element pick-ups resulted in the three-phase trip that had in fact occurred. The manufacturer also indicated that correct phase selection is guaranteed for all faults with actual fault resistance up to 10 ohm secondary, with the fault detection polygon set as per the 7SA513 relay performance guarantee document [21].

Correct directional determination is furthermore guaranteed under the following circumstances [Appendix M]

- Overall transmission angle of the system (generator angles) should be $\leq 60°$ with a relay setting along the R-axis $\leq 20\ \Omega$ secondary.
- With smaller transmission angles, larger R-axis settings can be tolerated.

A non-directional decision has the same significance and reaction as a reverse decision, whilst a non-directional decision cannot occur for a forward fault.

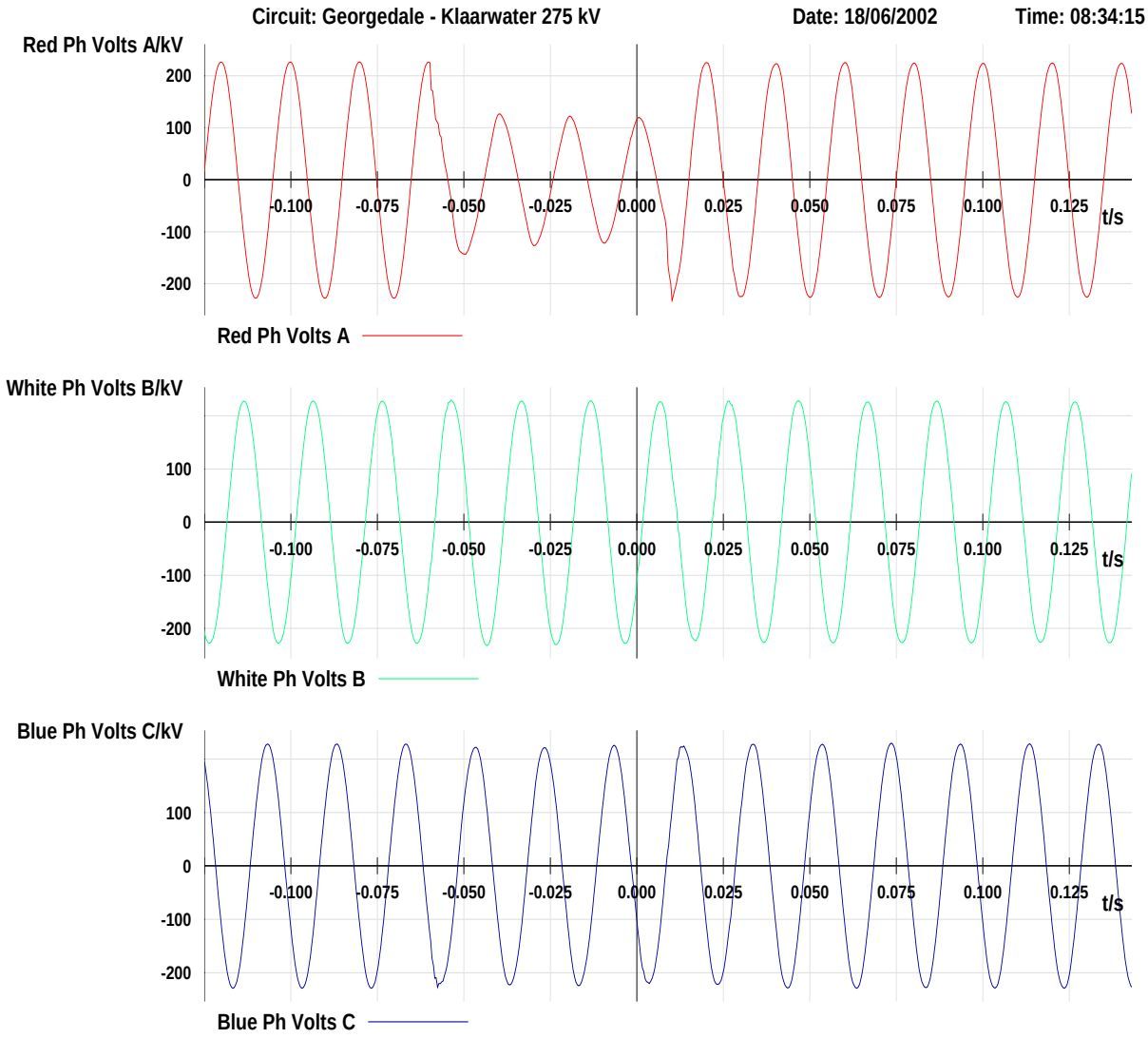

Figure 5.20: Voltage traces for Georgedale - Klaarwater 275 kV feeder

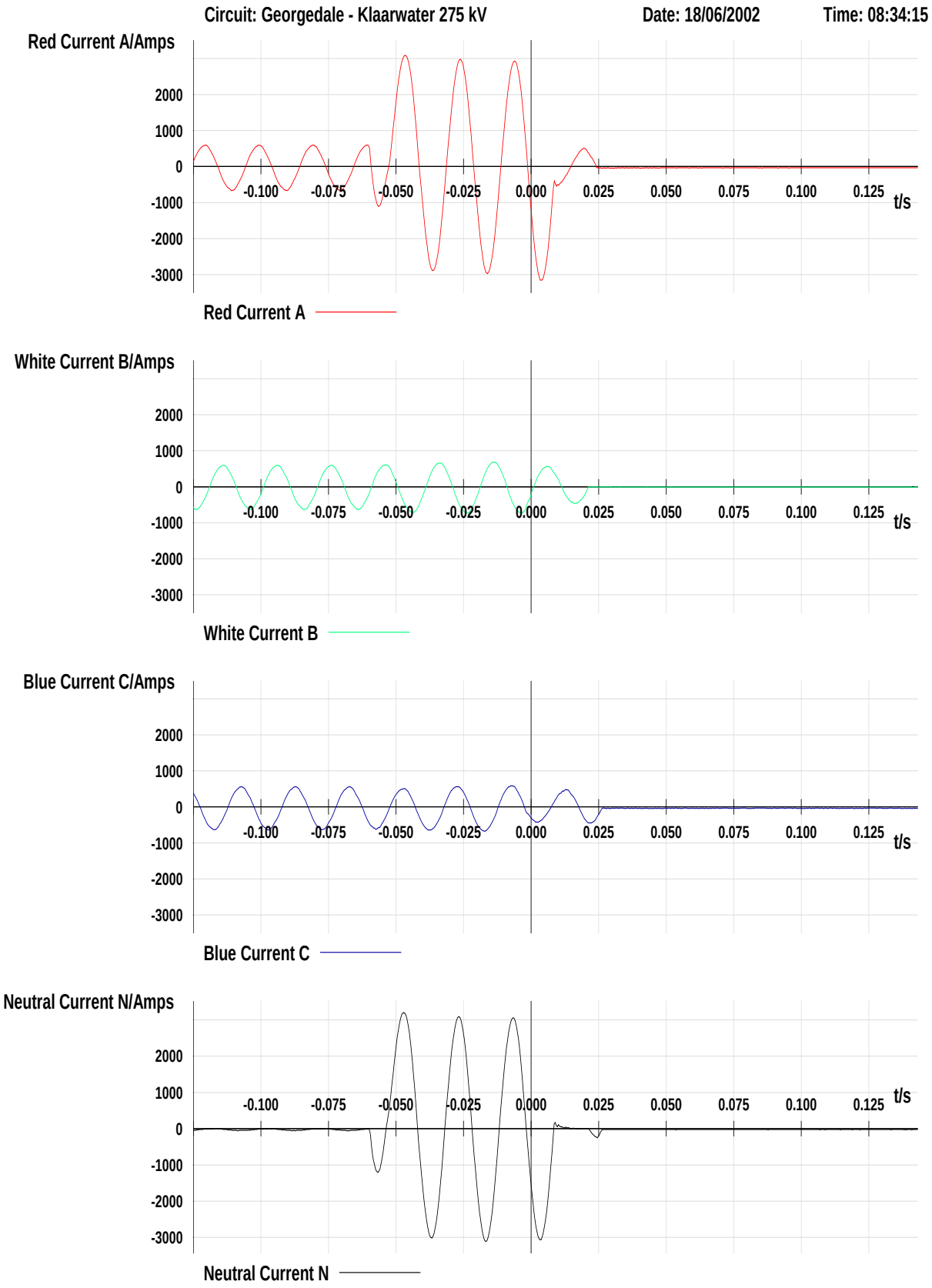

Figure 5.21: Current traces for Georgedale - Klaarwater 275 kV feeder

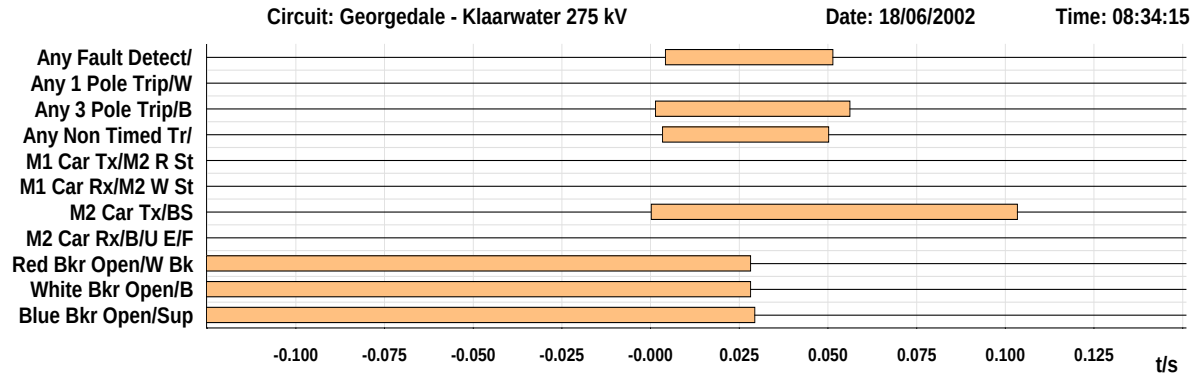

Figure 5.22: Binary traces for Georgedale – Klaarwater 275 kV feeder

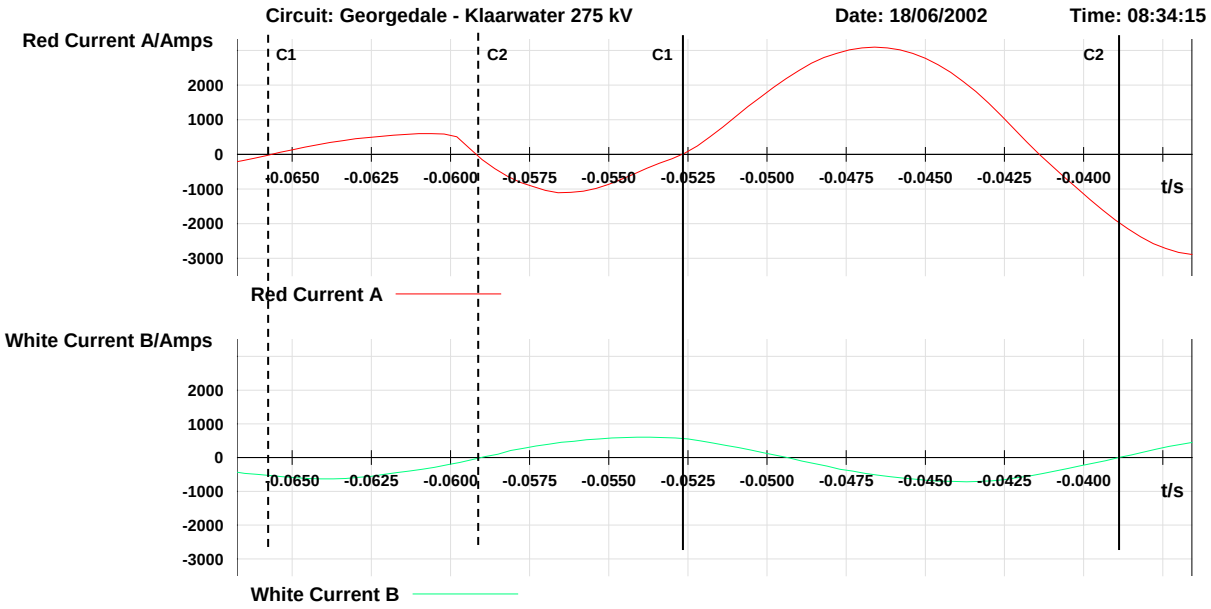

Figure 5.23: A and B-phase current angular comparisson

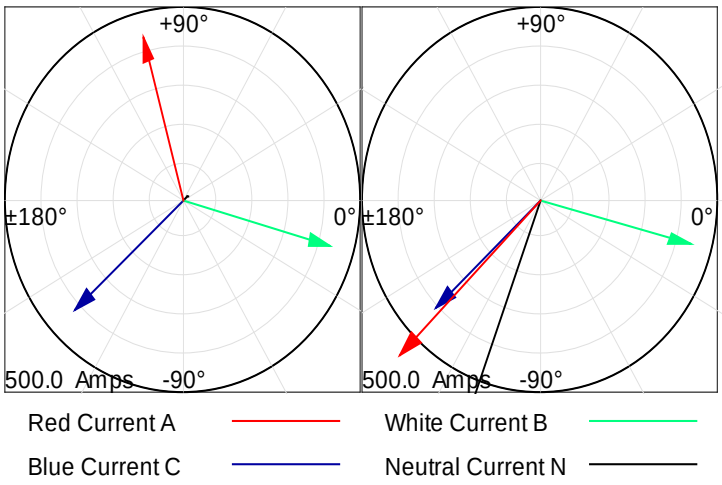

Figure 5.24: Current vector diagrams before and during the A-phase fault

Figure 5.25 illustrates the C-phase overreaching the relay zone 1 characteristic on the resistive axis.

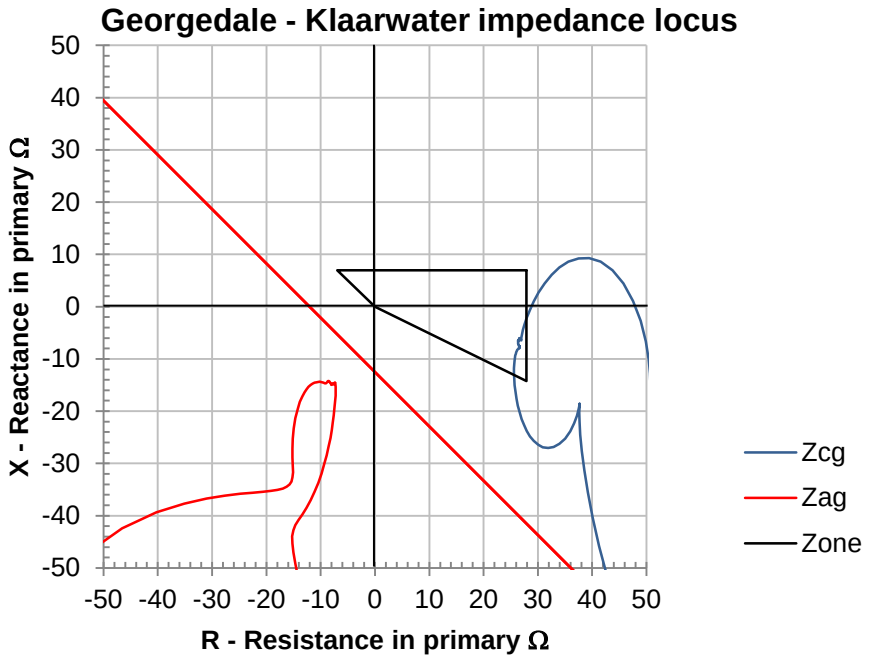

Figure 5.25: Georgedale - Klaarwater impedance locus at time of fault

Based on the above and knowing that the resistive setting was set at 27.89 Ω, it raised questions about the extent to which this setting exceeded the limitation of 10 Ω for correct phase selection. It was obvious that in order to prevent such an occurrence from happening again, the relay settings had to be altered. Question was by how much should the resistive reach be reduced, why it was necessary in the first place and would there not be other system fault conditions for which the same could happen again. This will be further explored in section 5.8.

5.5 Etna – Taunus faults analysis

5.5.1 Incident

An A-phase-to-earth fault occurred on the 10th of October 2000 at 03:50:37 on one of the 88 kV feeders feeding from Etna substation. The relevant 88 kV feeder protection correctly operated and cleared the fault in zone 1 time. The Etna – Taunus 275 kV feeder tripped in sympathy, incorrectly operating for the same fault.

5.5.2 Investigation and findings

The Etna – Taunus line is a short line, 18.56 km in length with a positive sequence impedance of $Z_1 = 0.3453 + j4.447\ \Omega$ and zero sequence impedance of $Z_0 = 5.636 + j20.239\ \Omega$. An A-phase-to-earth fault occurred on an 88 kV outgoing feeder from Etna substation. The voltage and current recordings shown in Figure 5.26 and Figure 5.27 indicate an A-phase-to-earth fault lasting approximately 4 cycles. The C-phase trip as indicated by the C-phase current in Figure 5.27 can be explained with the help of Figure 5.31.

Figure 5.31 shows that the unfaulted C-phase impedance locus enters the relay's zone 1 impedance characteristic in the first quadrant resulting in the blue-phase trip. Cursors (C_1) and (C_2), shown in Figure 5.29, indicate the fault clearance positions for the unfaulted Etna – Taunus 275 kV feeder and the faulted 88 kV feeder respectively, whilst cursor (C_0) indicates the position of fault inception. The unfaulted Etna – Taunus feeder C-phase breaker was open in 59.33 ms, whilst the faulted 88 kV feeder, only had the A-phase breaker open after 79.69 ms clearing the fault.

It was found that binary traces for Direct Transfer Trip (DTT) Receive, Breaker unhealthy, A and B-phase breaker poles shown in Figure 5.28 were in fact faulty, therefore providing misleading information. Figure 5.27 shows that only the C-phase breaker pole tripped and reclosed after approximately 1 s. Figure 5.30 gives a vectorial representation of the currents seen by the Etna – Tuanus feeder. The change in relationship between the vectors is similar to that previously described for the Georgedale – Klaarwater incident, therefore also indicating a reverse fault. It was concluded that the 88 kV feeder protection had in fact operated correctly, and that the protection on the 275 kV Etna – Taunus feeder should not have operated for the 88 kV fault. The resistive settings on this line were found to be excessive in relation with the reactive reach. The R/X-ratio, as set on the relay, was found to be greater than 9. With the 7SA513 relay's loop correction factors K_r and K_x of 6.11 and 2.19 respectively the R/X-ratio in the loop domain was calculated to be 23.06. This is rather excessive when compared to the maximum allowable R/X-ratio of 6.

No other deviation from allowable setting ranges and/or equipment failures was found, and therefore it was concluded that the excessive resistive reach and the corresponding R/X-ratio used in the settings was the root cause for the Etna – Taunus relay maloperation for this fault. The setting changes to be implemented will be discussed in section 5.8.

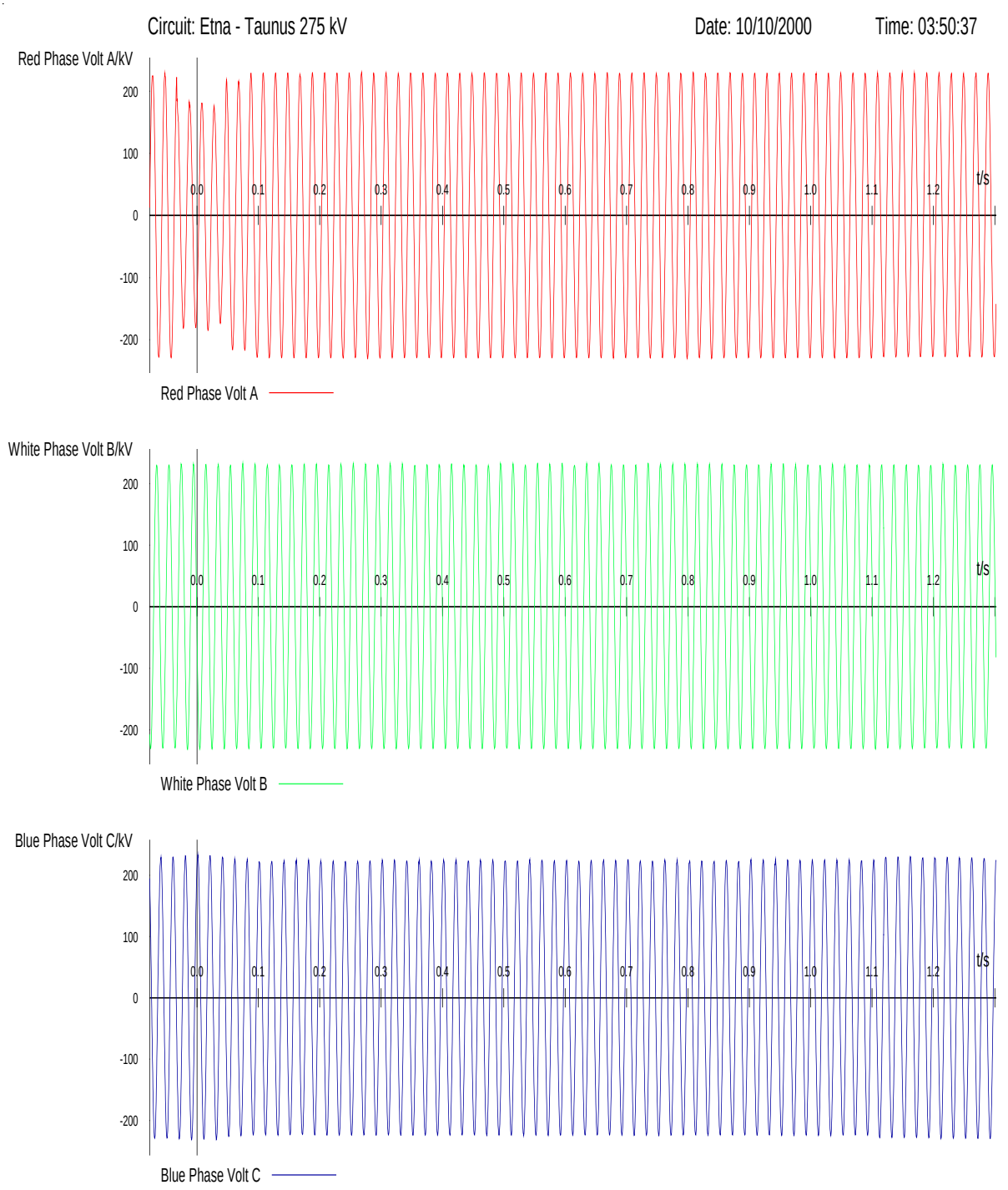

Figure 5.26: Voltage traces for Etna - Taunus 275 kV feeder

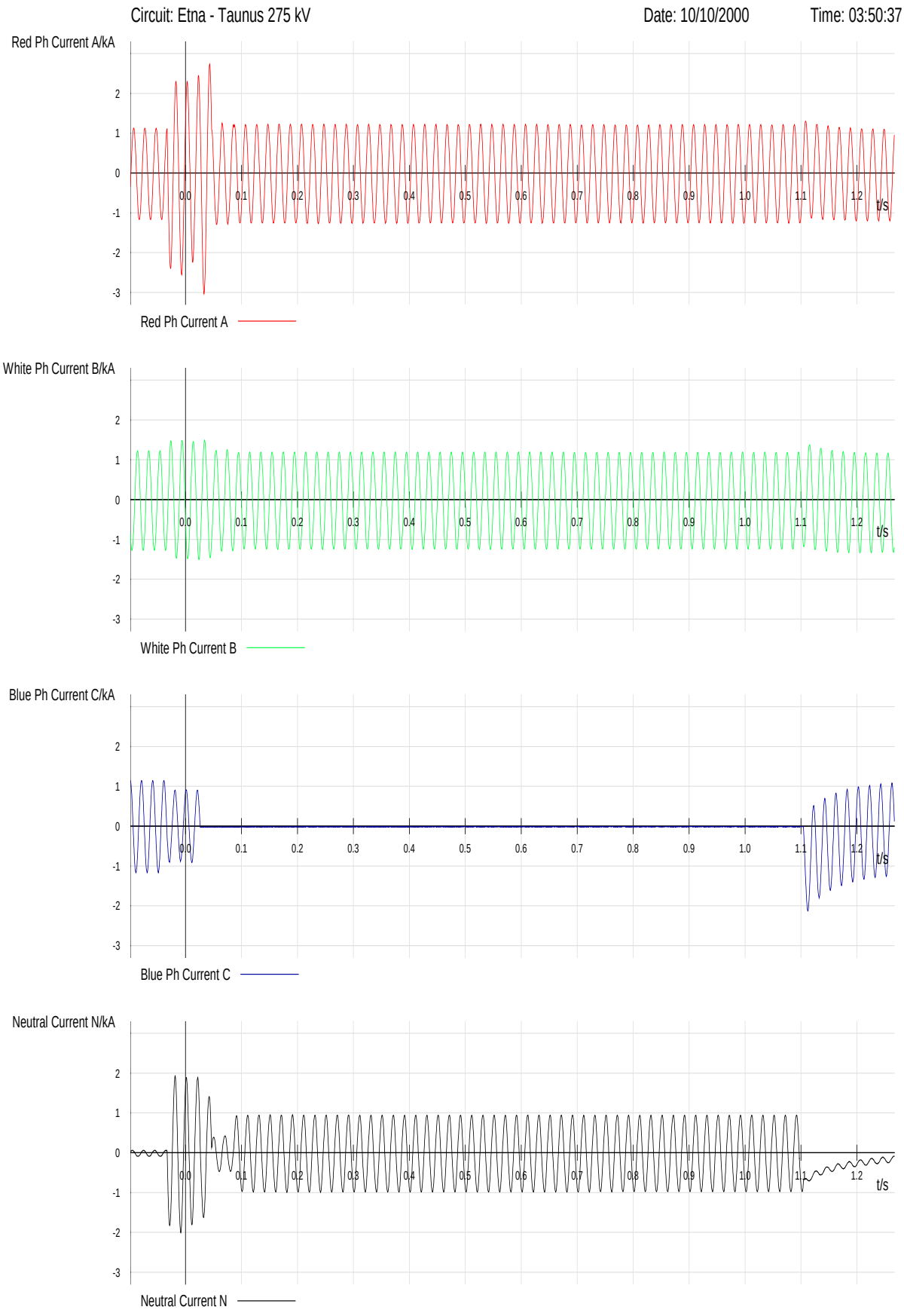

Figure 5.27: Current traces for Etna - Taunus 275 kV feeder

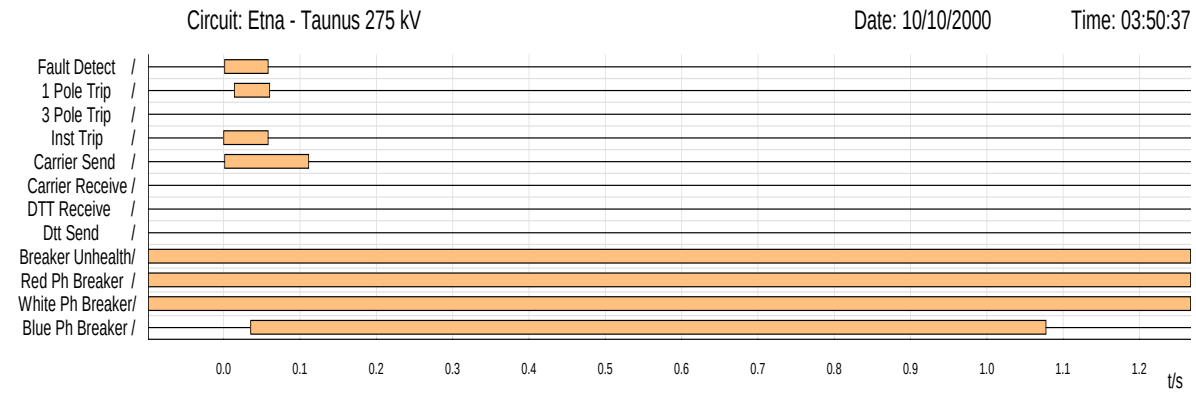

Figure 5.28: Binary traces for Etna - Taunus 275 kV feeder

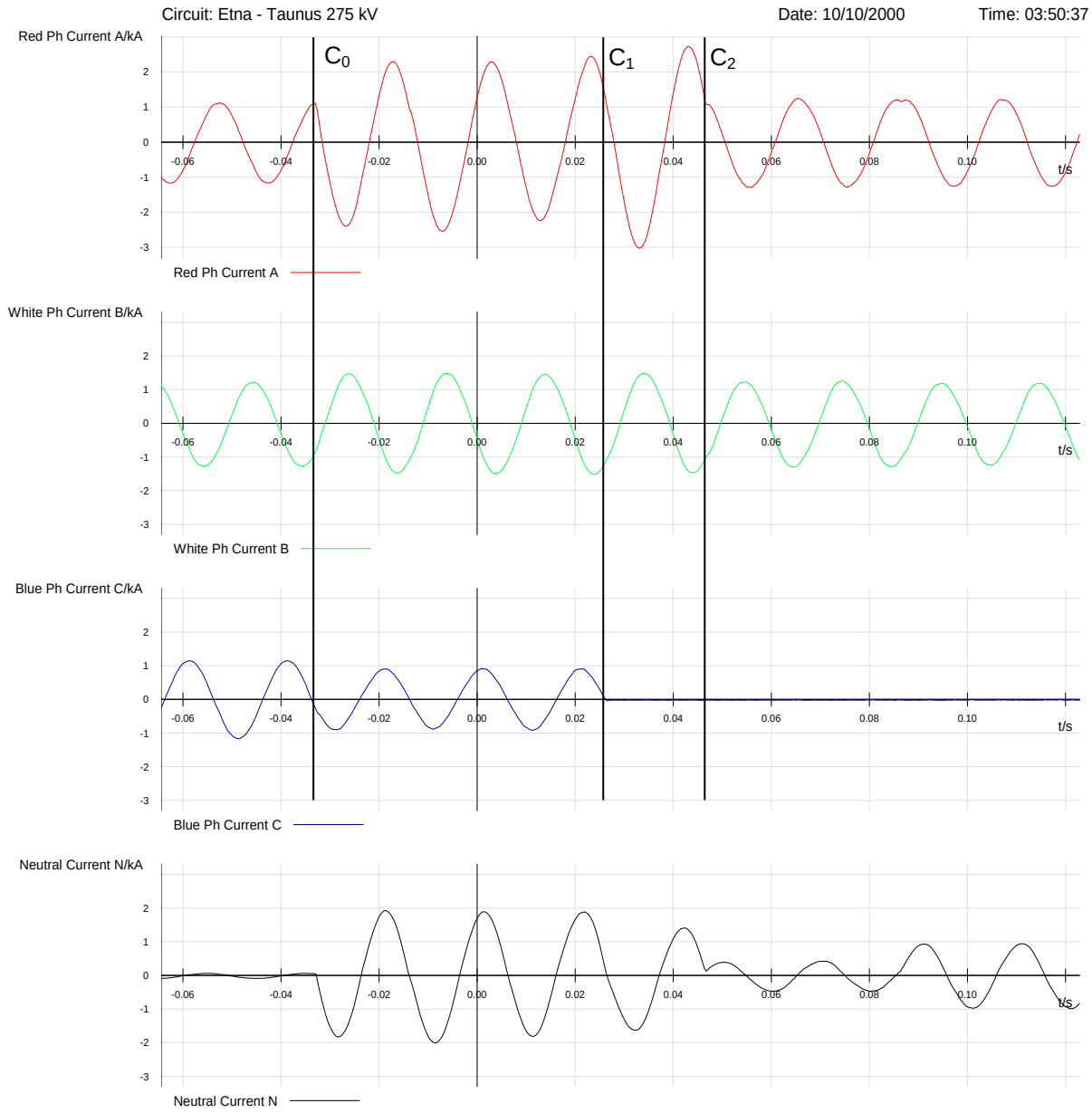

Figure 5.29: Etna - Taunus 275 kV enlarged current traces

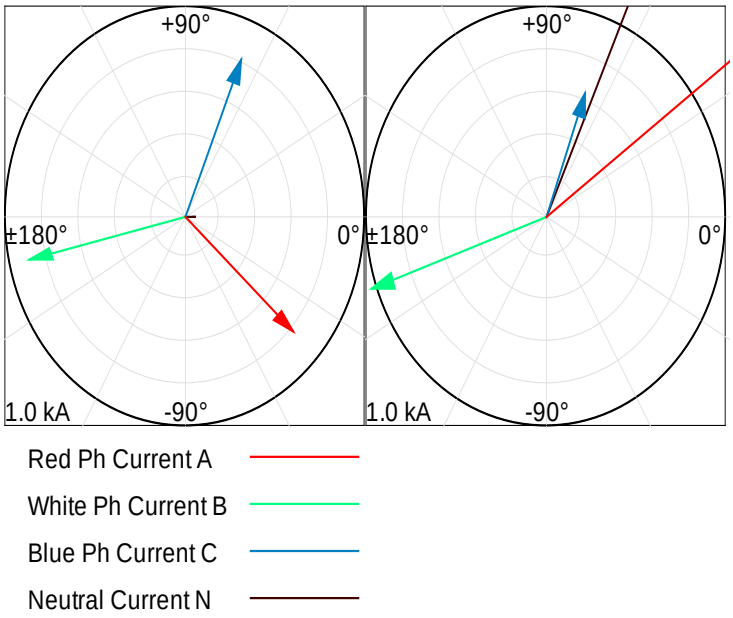

Figure 5.30: Etna - Taunus 275 kV current vector diagram

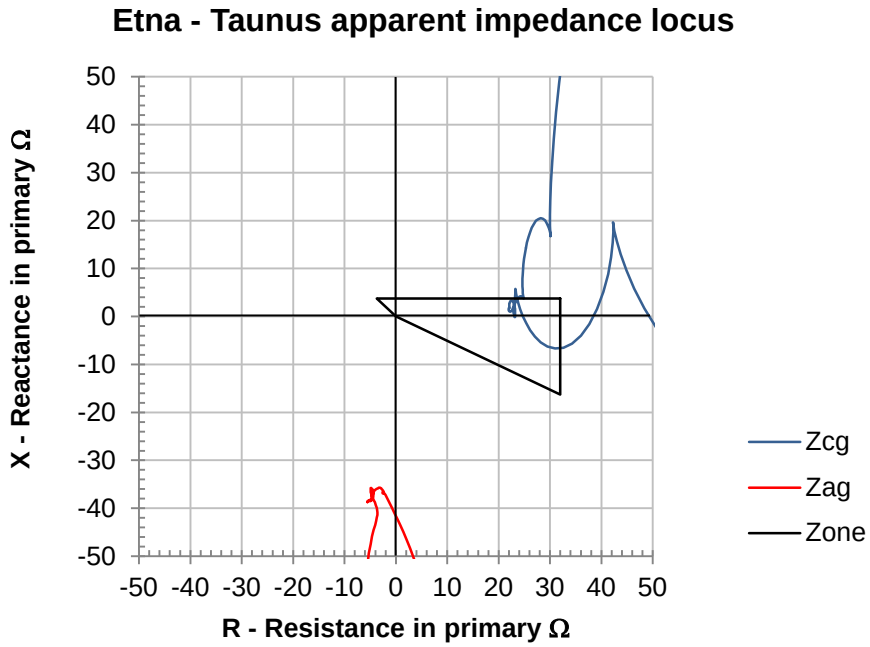

Figure 5.31: Etna - Taunus 275 kV fault impedance locus before changes

5.6 Bacchus – Droërivier fault analysis

5.6.1 Incident

A B-phase-to-earth fault occurred on the 14th of April 2010 at 02:30:10 pm on the Baccus – Droërivier 400 kV line. The protection at both ends were slow in operating as can be observed from the fault recording shown in Figure 5.32. Considering the fact that the protection in service is of the new numerical type, this raised concerns in terms of all aspects relevant to the commissioning process.

5.6.2 Investigation and findings

The Bacchus – Droërivier line is a mid-section series compensated line with an overall length of 401.78 km. The feeder has positive and zero sequence impedances of $Z_1 = 10.66 + j127.86\ \Omega$ and $Z_0 = 123.9 + j436.72\ \Omega$ respectively. The CTR has been selected as 1600/1 whilst Twin Dinosaur phase conductor is used. The voltage and current traces shown in Figure 5.32 indicate an original B-phase-to-earth fault that was only cleared at the Bacchus end after approximately 1.4 s.

A sharp increase in the red and C-phase voltages can be seen at this point together with an even greater decrease in voltage on the B-phase, highlighting the already known fact that a B-phase-to-earth fault occurred. The fault is finally cleared at around 2.67 s after fault inception.

For the purpose of this document we will focus on the events at Bacchus substation only. Superimposing the red, white and neutral currents reveal that all three currents are almost perfectly in phase during the fault, indicating that in fact a red-to-B-phase-to-earth fault occurred, with the A-phase current being the more dominant phase current.

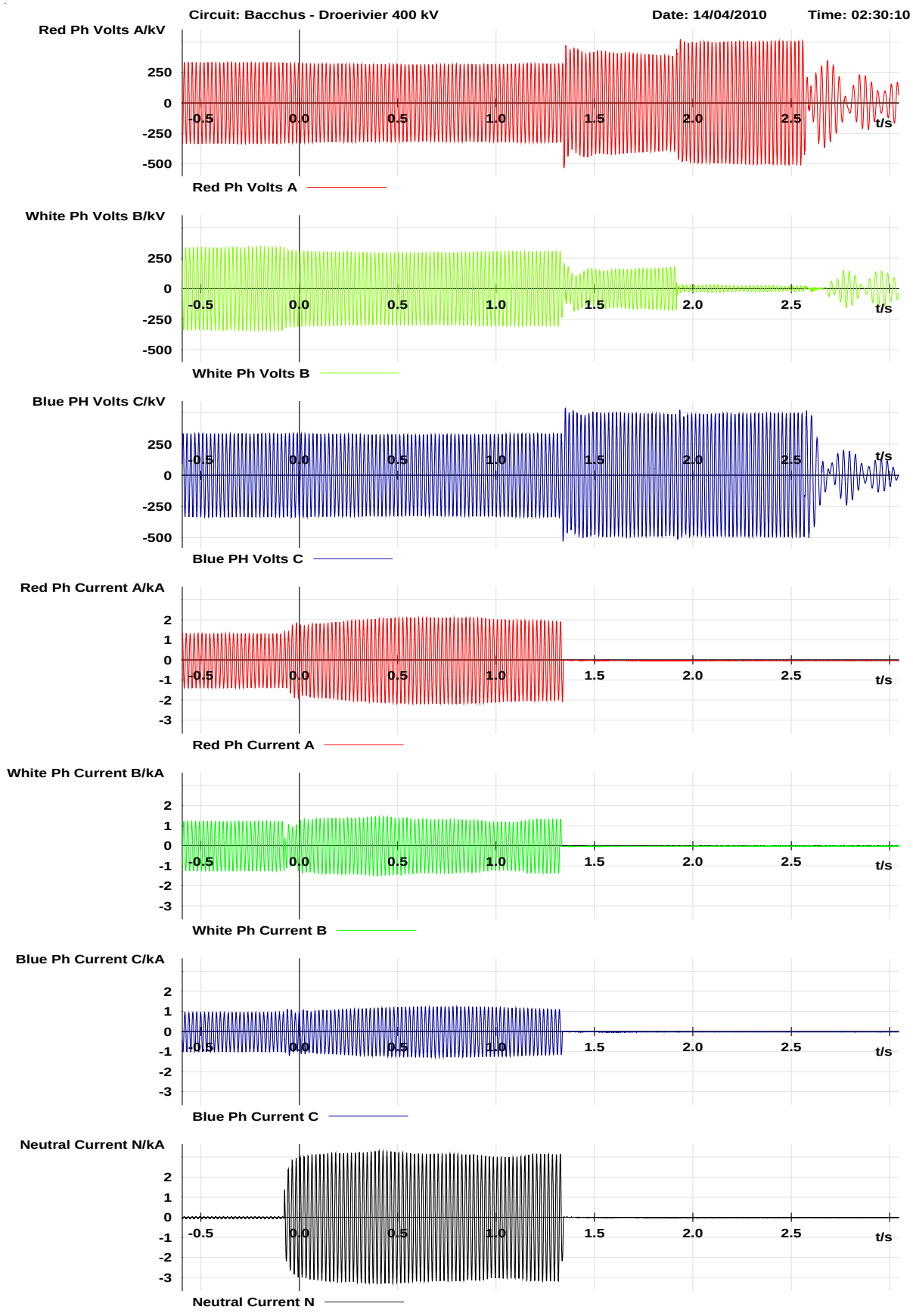

Figure 5.32: Bacchus - Droërivier voltage and current traces

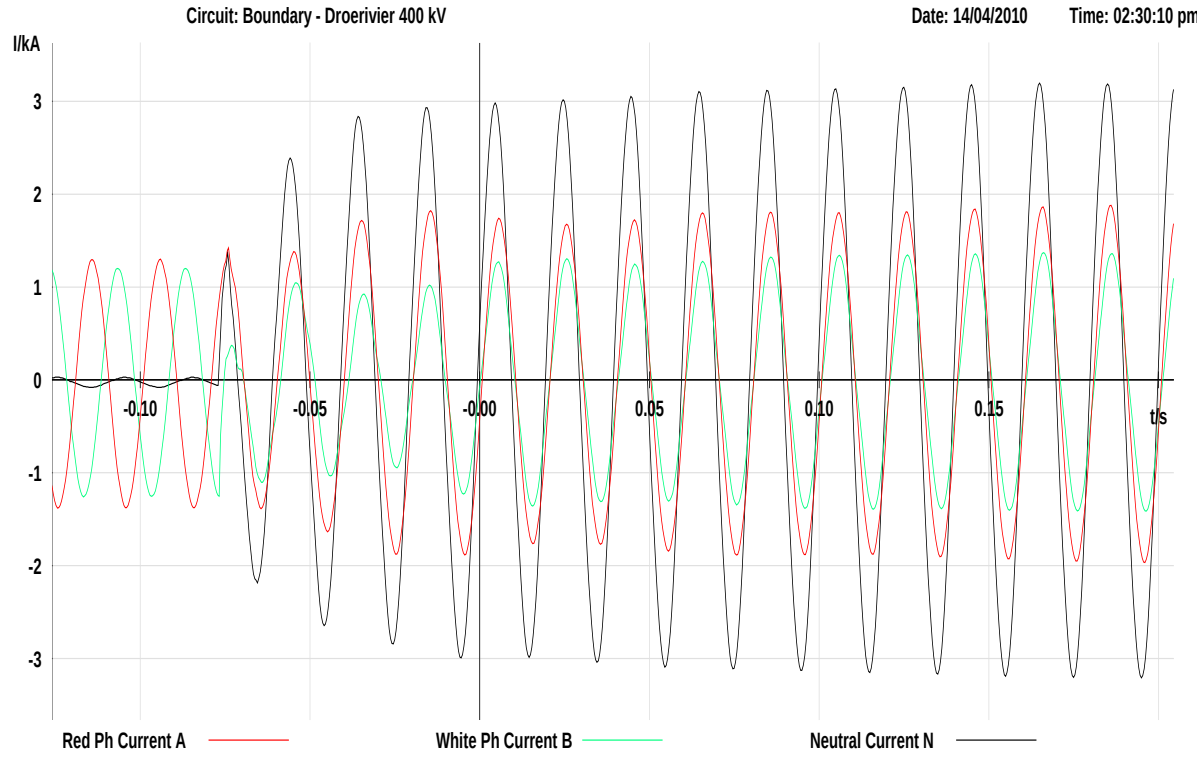

Figure 5.33: Superimposed fault currents on Bucchus - Droërivier feeder

The binary signals, shown in Figure 5.34 have been optimised to reflect only those elements that picked up. Figure 5.34 indicates that the relay's fault detection had picked up, but that tripping only occurred after the backup IDMT earth fault element operated. The relay's operating characteristics for the zone and phase selector measuring elements was then superimposed on the fault impedance locus and is shown in Figure 5.35.

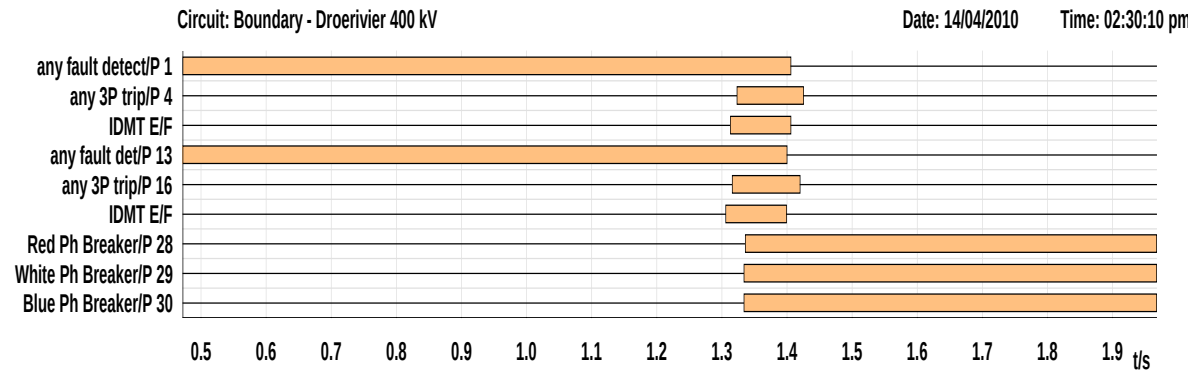

Figure 5.34: Bacchus - Droërivier binary signals

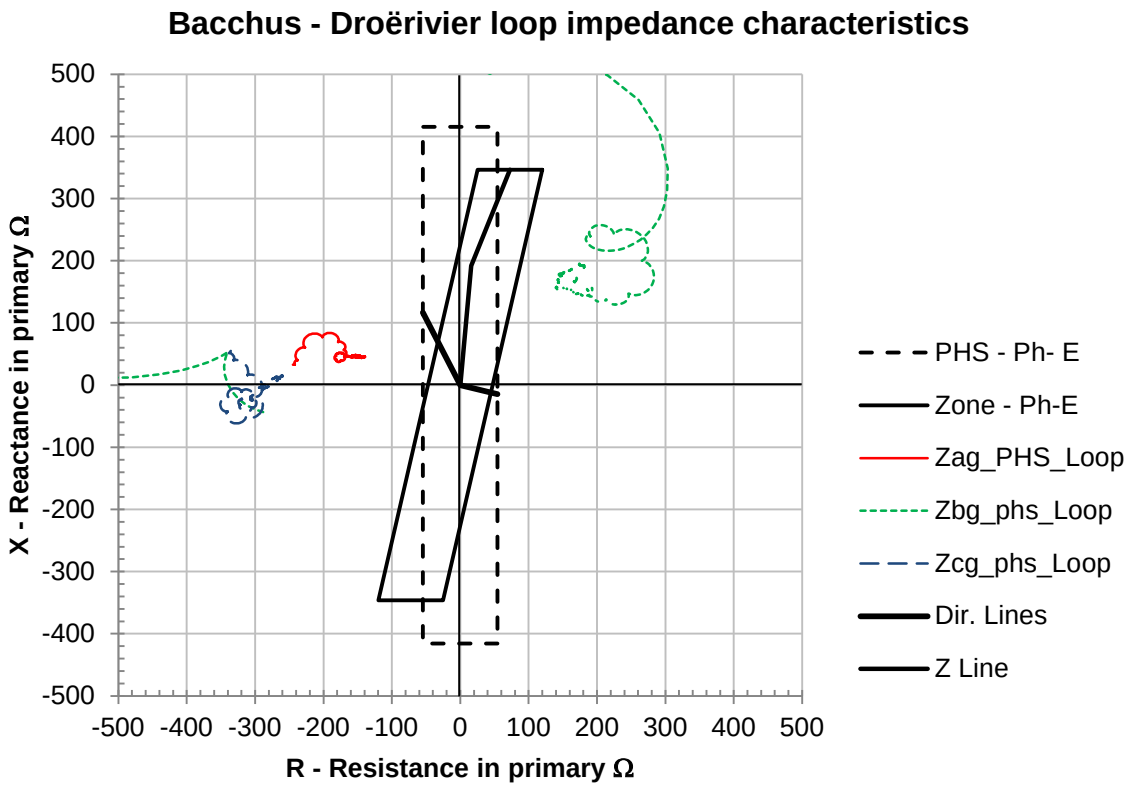

Figure 5.35: Bacchus - Droërivier phase-to-earth fault loop impedance

It can be shown that for the phase-to-earth loop impedances both the zone and phase selector measurements are identical. None of the phase–to-earth measuring loops enters either of the relay's set characteristics. Important to note at this point is that the phase selector characteristic does not cover the zone characteristic as shown in Figure 5.35, both plotted in the loop domain. The zone 2 phase-to-earth reach was set to Z_{2E} = 47.3 + 16 + j192 Ω (R_{FPE} + R_{1PE} + jX_{1PE}) in primary quantities providing an overall loop impedance of Z_{2_Loop} = 119.9 + j346.23 Ω/loop, where $Z_{2\_Loop} = Z_2 + Z_{2N} + R_F$. The phase selector settings had been set to R_{FPE} = 54.5 Ω/Loop, X_{1PE} = 230.16 Ω/phase and X_{0PE} = 786.1 Ω/phase in primary quantities. Although correcting the phase selector setting to encompass the zone characteristic would make no difference towards ensuring operation in this case, it is important to note that it is a criterion of the relay that the phase selector be set larger than that of the zone to ensure operation and correct phase selection.

The only option to properly cater for slow developing high resistive faults such as the fault under consideration, would be to employ a high sensitivity earth fault

comparison scheme. This type of scheme does unfortunately depend on the availability of a further communication channel. Since the fault information indicated a red-to-white-to-earth fault, the phase-to-phase loops were also evaluated and similar results as for the phase-to-earth fault loops were found. Figure 5.36 represents the phase-to-phase analysis of the fault impedance loops superimposed on the relay phase-to-phase loop impedance characteristic. The A-B-phase impedance loop is not shown since it is located far outside the range of the graph.

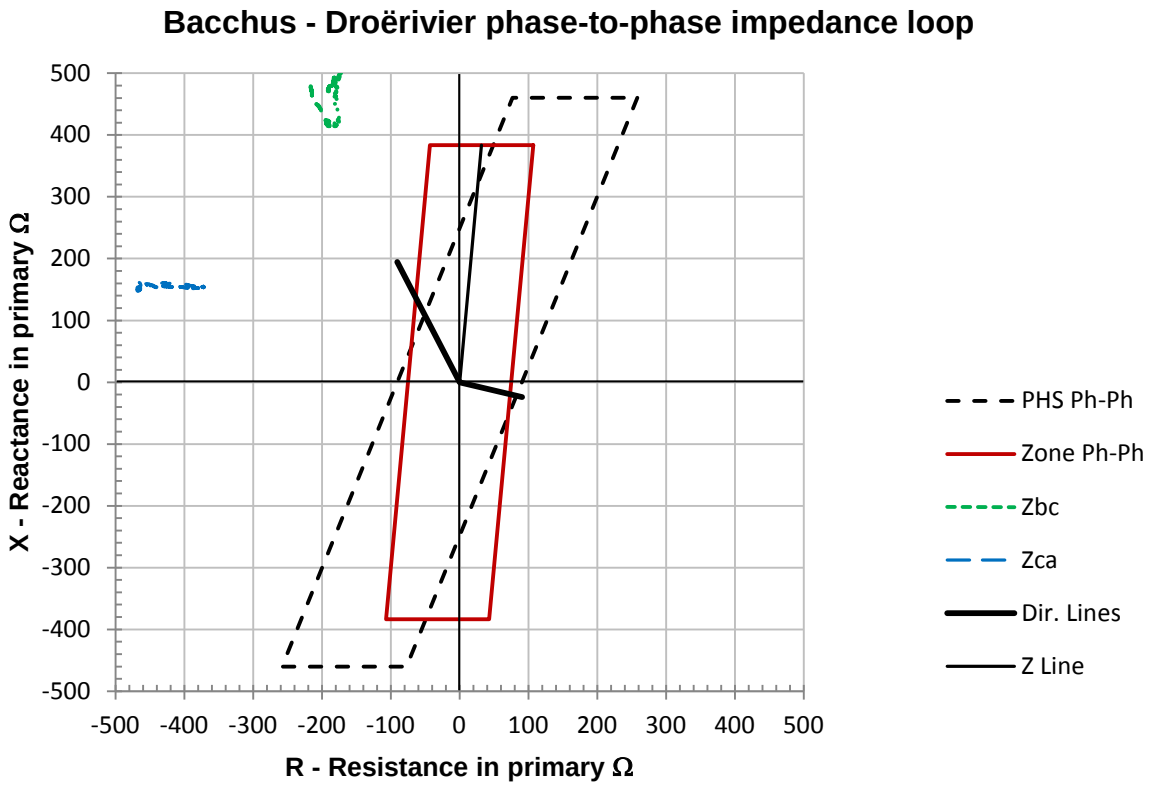

Figure 5.36: Bacchus - Droërivier phase-to-phase fault loop impedance

The required setting changes for the phase-to-earth elements will be discussed in detail in section 5.8.

5.7 Leander – Grootvlei fault analysis

5.7.1 Incident

An A-phase-to-earth fault occurred on the 30th of December 2008 at 04:39:56 pm on the Leander – Grootvlei 400 kV feeder. The A-phase breaker pole tripped and reclosed after approximately 1 s, restoring supply.

5.7.2 Investigations and findings

The Leander – Grootvlei feeder has an oveall length of 251.62 km, with positive and zero sequence impedances of $Z_1 = 6.7516 + j79.735\ \Omega$ and $Z_0 = 77.903 + j273.845\ \Omega$ respectively. The selected current transformer ratio (CTR) was 2000/1 whilst Twin Dinosaur conductor is used for the overhead phase conductor. The voltage and current traces shown in Figure 5.37 indicate an A-phase-to-earth fault that remains for 439.06 ms, before being cleared. The breaker reclosed after single-phase dead time of approximately 1.168 s. The only obvious concern is linked to the time duration of the fault. Under normal conditions a system fault should be cleared between 80 to 100 ms. Figure 5.38 and Figure 5.39 have been added for information purposes only to show the phase relationship between the A-phase and neutral during the fault. Figure 5.38 illustrates the phase shift in the faulted A-phase current that occurs at fault inception 57.8 ms prior to the recording trigger at 0 ms. The A-phase current is shown in Figure 5.39 shifted through approximately 105° during the fault.

The binary triggers shown in Figure 5.40 indicate main 2 carrier signal received after 57.86 ms with fault detection pickup only 79.06 ms after fault inception. An instantaneous trip pickup realises after 411.86 ms with a single-phase trip output been given at 431.06 ms after fault inception. The binary triggers only provided us with actual timed event information related to the fault, highlighting the long time duration of the fault, but failed to provide information of the cause of the long fault duration.

The relay's zone 1 characteristic for the phase-to-earth loop is shown superimposed on the fault impedance locus in Figure 5.41. All quantities have been plotted in the loop domain, and can therefore be compared directly. The graph shows that the phase selection characteristic is in fact set short of the zone characteristic in the resistive plain, causing the zone element to detect the fault whilst the phase selector did not. The phase selector function is crucial in determining how the relay operates. It is a requirement of the REL531 relay that the phase selector function picks up correctly for all fault loops on the line being protected, and determines the successful outcome of correct faulted phase selection and subsequent auto-reclose selection. Phase selection for this relay is done by impedance measurement for the first two zones and is always a loop impedance measurement [20]. This again highlights the importance of comparing the zone and phase selector elements in the same (loop) domain.

It was also found that the weak in-feed function on the relay had been switched off. The voltage only dropped to approximately 74.6% (245 kV/327 kV, peak) of Vnom (nominal voltage) during the fault, whilst the recorded neutral fault current reached a peak value of 2.37 kA. The ratio of RMS current as a factor of Inom is given by 2.37 kA/($\sqrt{2}$ * 2000) = 0.68. The neutral current therefore easily exceeds the required 10% of Inom (nominal current) required by the relay to release phase-to-earth measurement [20]. The weak in-feed requirement for an under-voltage and under-current condition is therefore not satisfied in this case.

The power swing detection function which is set in positive sequence quantities was compared to the phase-to-earth fault zone elements in the positive sequence domain, shown in Figure 5.42. The A-phase-to-earth (Z_{ag}) impedance locus crosses the power swing detection outer and inner characteristics for a time duration of approximately 1.2 ms (647.2 ms – 646 ms). Although this time is less than half the set 4 ms on the relay, one could argue that should a different cosine filter be used to extract the impedance parameters from the raw-data file, a different result could have been achieved. The exact filter and/or filters used by the relay manufacturer are not known. The cosine filter that was used in this analysis managed to highlight

specific shortcomings in the relay settings that was applied and can therefore be used to evaluate relay operations at this level.

Due to the fact that conclusive evidence could not be obtained with regards to the impact that the power swing blocking function might have had on this event and given the focus of this research, this aspect is left for further investigation. It has however been established that the zone and phase selector reaches in the resistive direction had not been set adequately, and needs to be revised. This will be discussed further in section 5.8. The impedance measurement for the power swing detection function of this relay is furthermore done on a per phase basis, and a selection of one out of three or two out of three loops can be made [20].

It was not clear as to what selections were made, since this is not relay setting, but rather relay logic related. It also falls outside the scope of this research and was therefore not pursued any further. It does however remain a possible reason for maloperation of the relay and should be investigated.

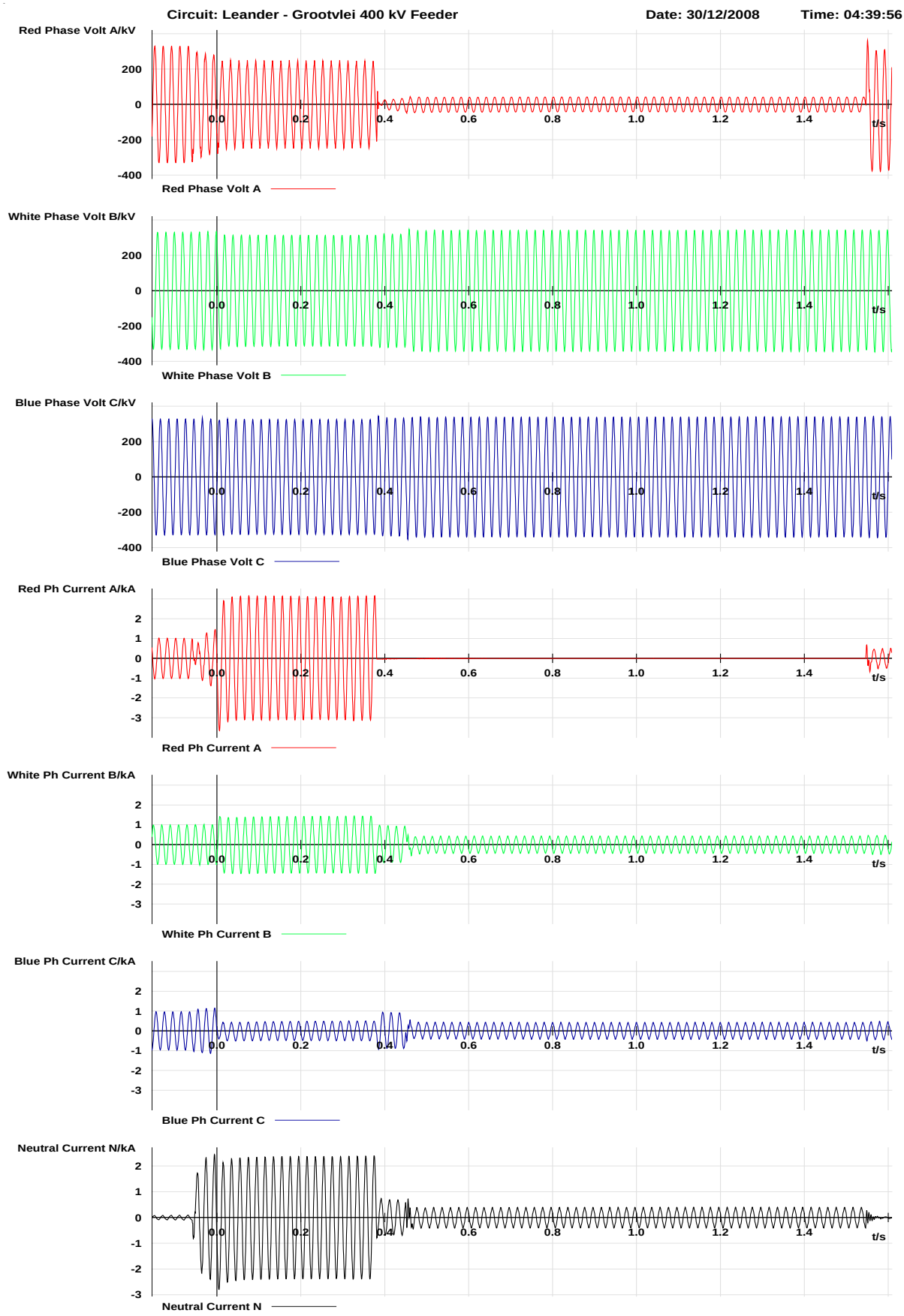

Figure 5.37: Leander - Grootvlei 400 kV Feeder voltage and current fault traces

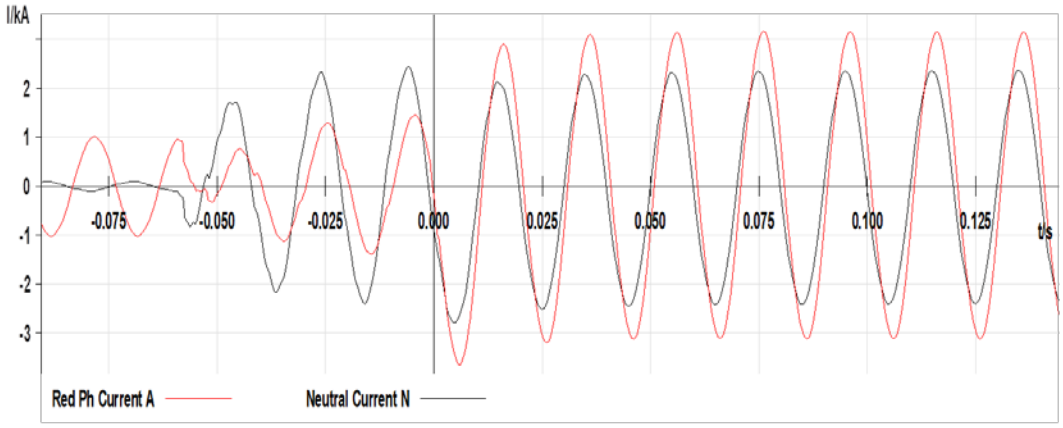

Figure 5.38: Leander - Grootvlei red and neutral currents

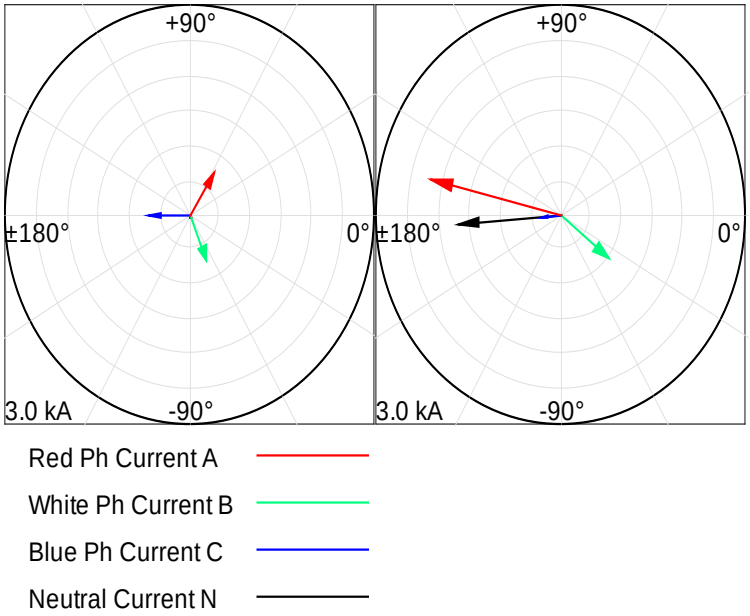

Figure 5.39: Leander – Grootvlei current vectors prior and during the fault

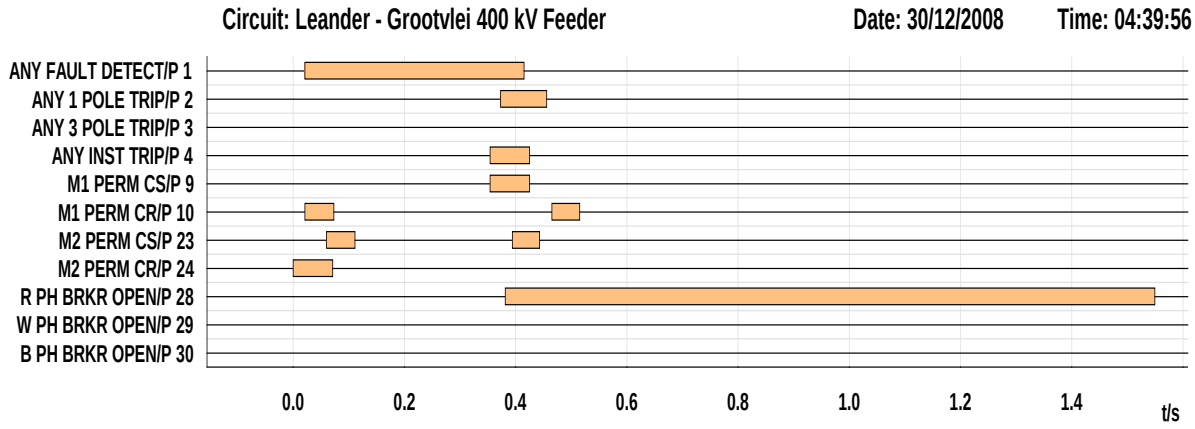

Figure 5.40: Leander - Grootvlei binary trip signals

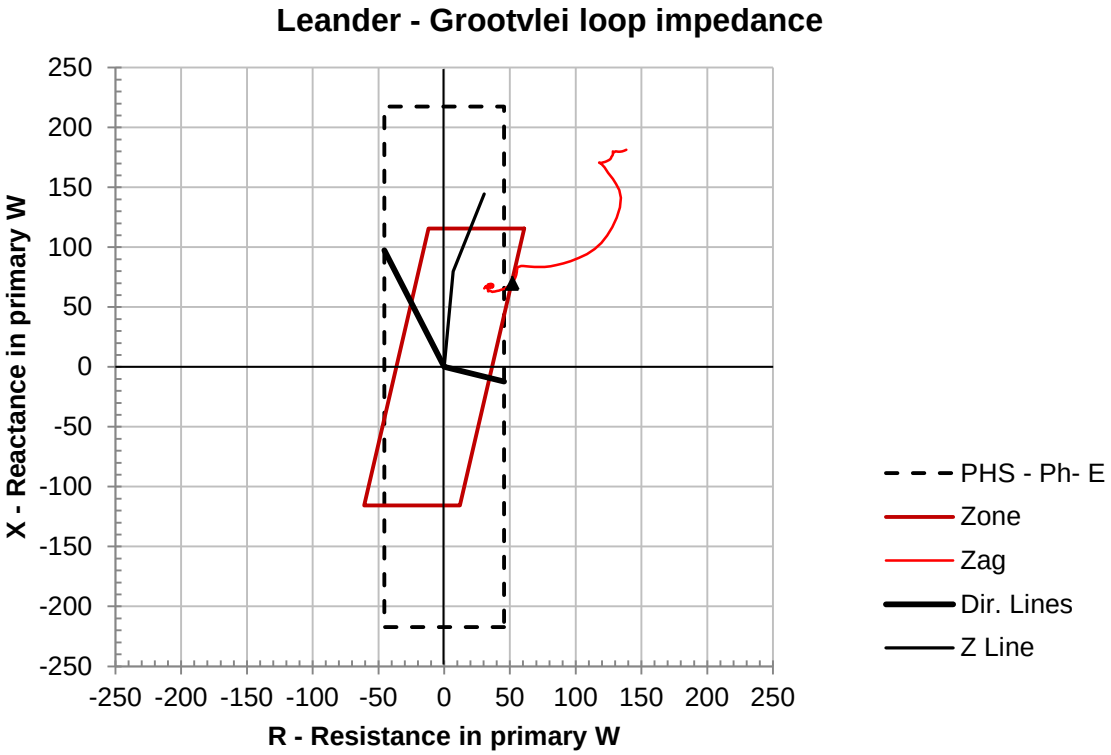

Figure 5.41: Leander - Grootvlei 400 kV phase-to-earth fault loop impedance

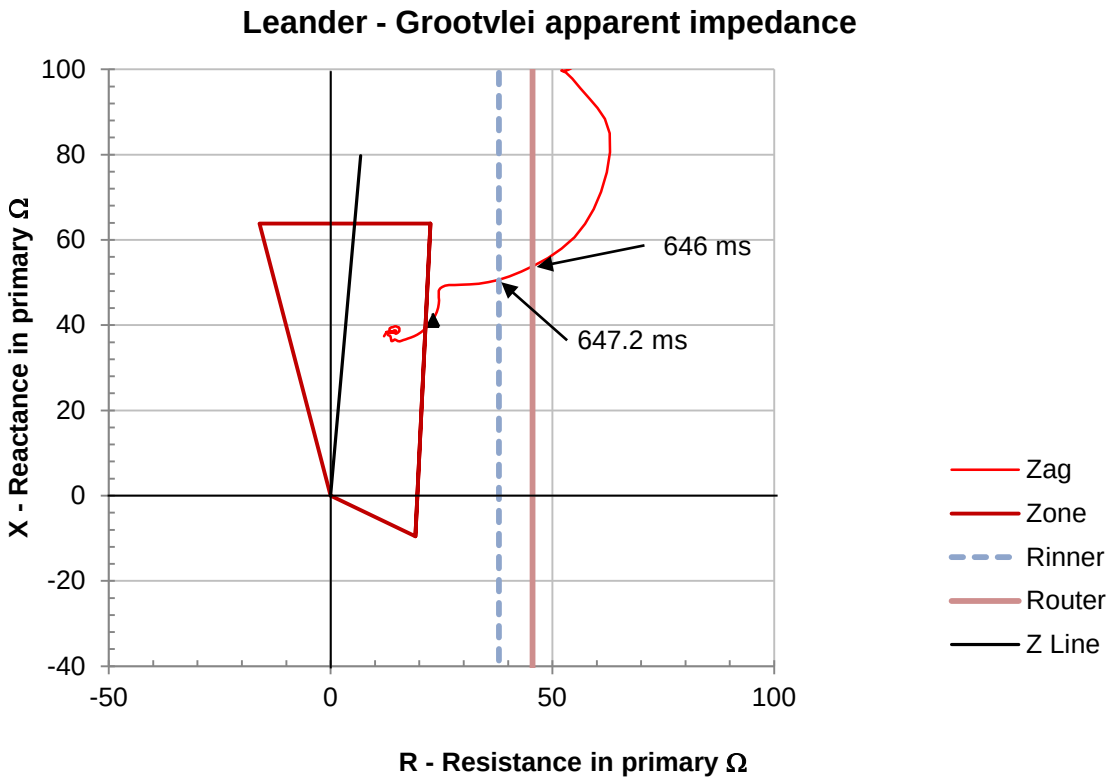

Figure 5.42: Leander - Grootvlei 400 kV phase-to-earth fault apparent impedance

5.8 Relay setting changes

The originally applied settings have effectively been set according to Siemens guarantee document SA513PG1.doc of 04 November 1994 (see Appendix M). These guarantee limitations were provided around Eskom's required performance for this relay, and included "example" settings for long, short and series compensated lines.

Secondary injection testing methods, allowing for play-back of the actual fault events, were used by field staff in all cases (discussed in the following sections) to test the newly calculated settings. The relays did not operate during fault play-back, which suggested that the maloperation problem had been resolved. All graphs represented shows the actual recorded fault events. The graphs shown in sub-sections 5.8.1 to 5.8.6 therefore show the actual recorded fault events superimposed on the corrected relay reaches. Binary traces of relay non-operation during fault play-back were not saved by field staff and are therefore not available to validate non-operation.

5.8.1 Athene – Invubu 400 kV line

The results obtained from the measurements and subsequent re-calculated impedance parameters, discussed in section 5.2.3.4 provided a definite cause for the relay maloperation that occurred. Using the relay theory discussed in chapter 3, we can determine the overall loop impedance that the relay was set to at the time of fault. Zone 1 was set to the normal 80% ($Z_1 = 0.543 + j5.62\ \Omega$) of the originally calculated line reactance, with a resistive coverage (R_F) of 21.21 Ω, given in primary values (VTR = 400 kV/110 V and CTR = 2400/1). With the measured line impedance of $Z_L = 0.587 + j7.128\ \Omega$ (section 5.2.3.4 refers) it seemed unlikely to cause any reactive overreaching problem.

The measured zero sequence impedance holds the key to this problem. Considering the same relay reach, but evaluated in the loop domain we find that with the original calculated zero sequence impedance values of $Z_0 = 6.702 + j23.825\ \Omega$ the matching earth impedance factors K_r and K_x was calculated to be 4.78 and 1.8

respectively. This results in an overall set loop impedance of $Z_{1Loop(sett)}$ = 101.47 + j10.116 Ω, inclusive of the fault resistive coverage (R_F). (21.21 * 4.78 + j 5.62 * 1.8).

The reactive loop reach set on the relay is slightly larger than the actual reactive loop value of the line, effectively providing a zone 1 reach of 100,1% that resulted in the Athene – Invubu relay maloperation. A contradiction was found between the R/X-ratios allowed for in the 7SA513 relay settings guidelines and that in the relay manual. The relay manual allows for a maximum R/X-ratio $_{(sett)}$ of 6, which seems to relate to the actual applied setting ratio. Impedance fault detection is however a loop dedicated fault detection procedure, also explicitly stated by the manufacturer, which is a definite indication that not the actual setting on the relay but the overall loop relationship must be used in determining the R/X relationship.

The ratio of actual values set on the relay $R_{1(sett)}/X_{1(sett)}$ was compared to the calculated loop values $R_{1Loop(sett)}/X_{1Loop(sett)}$. Values of 3.77 and 10.02 were respectively obtained. Since the loop ratio exceeded the specified relationship of 6 this provided yet another reason as to why the relay had in fact operated for the fault on the remote end busbar. Normal practice would be to reduce the reactive reach to values less than 80% in cases where this ratio relationship needs to be exceeded for adequate fault resistive coverage. The relay settings was revised and new zone 1 reach of Z_1 = 14.77 + j5.7 Ω, with R_E/R_L and X_E/X_L ratios of 2.27 and 0.42 respectively applied. These new settings also provided R/X-ratios of 2.59 and 5.96 in the as set and loop relationships respectively, providing an overall loop impedance coverage of Z_{1_Loop} = 48.29 + j8.09 Ω. Note the reduction in both the resistive and reactive coverage, with the most significant reduction in the resistance. Adequate resistive coverage is still achieved for zone 1 reach. The CT-ratio was also changed 1600/1 thereby enhancing the overall measurement sensitivity in the event of high resistive faults.

Figure 5.43 represents the impedance locus superimposed on the positive sequence or apparent impedance plane after the new settings had been implemented. The impedance locus now does not enter the relay characteristic. It is therefore clear

that the reactive setting on the relay was never incorrect, but rather the X_E/X_L setting on the relay. The set value of R_E/R_L was also changed to ensure that the R/X-ratio as seen in the loop domain does not exceed the value of 6.

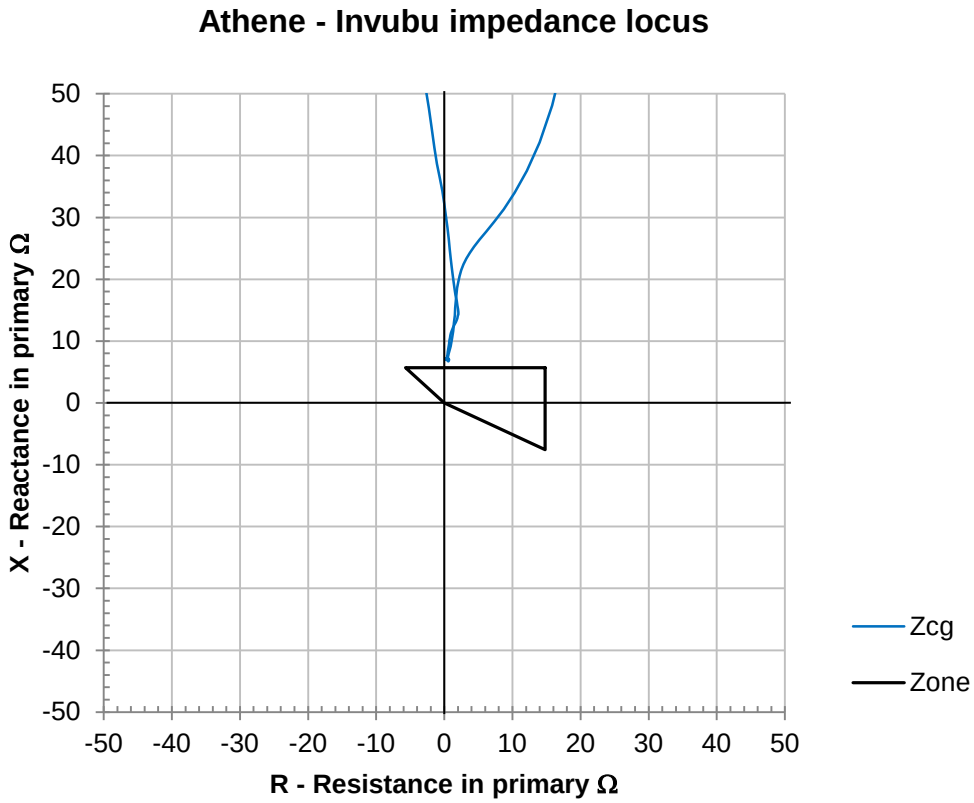

Figure 5.43: Athene - Invubu impedance locus after setting changes

For the sole purpose of completeness, the R/X relationship before and after setting correction is graphically shown in loop impedance representation in Figure 5.44 and Figure 5.45. The reactive overreach and the extensive resistive coverage as set on the relay at the time of fault are clearly visible in Figure 5.44, whilst the impact of the setting changes for both reactive and resistive reaches are also apparent when comparing these figures.

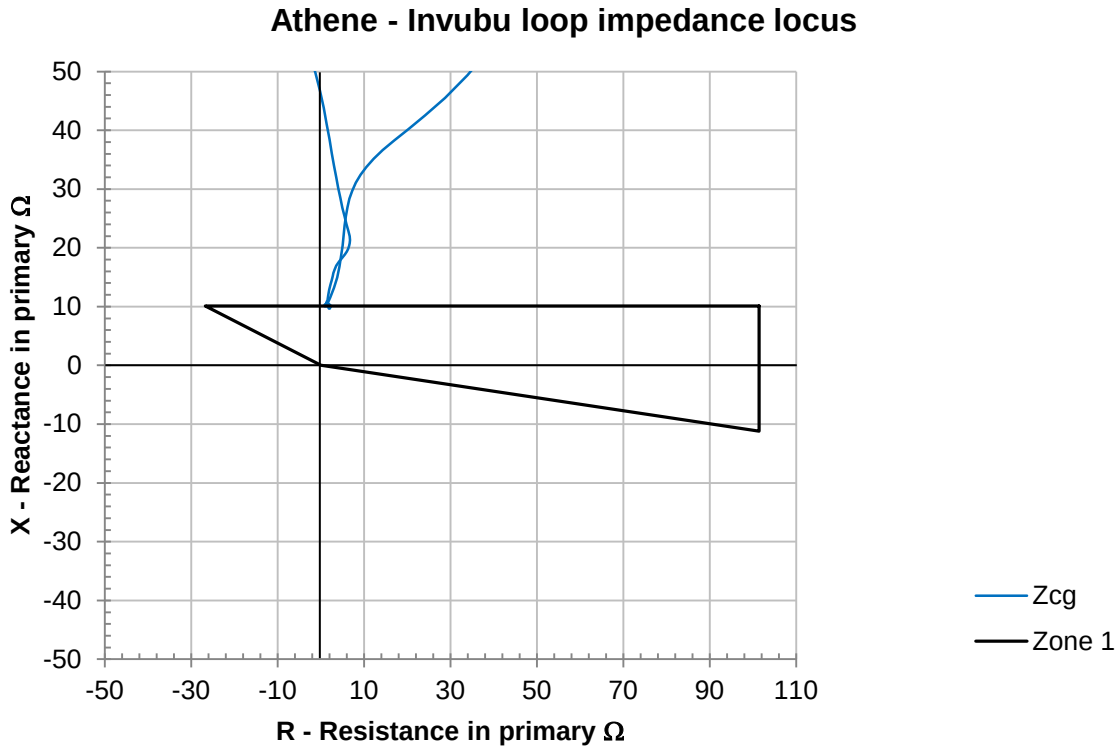

Figure 5.44: Athene - Invubu impedance loop relationship (before)

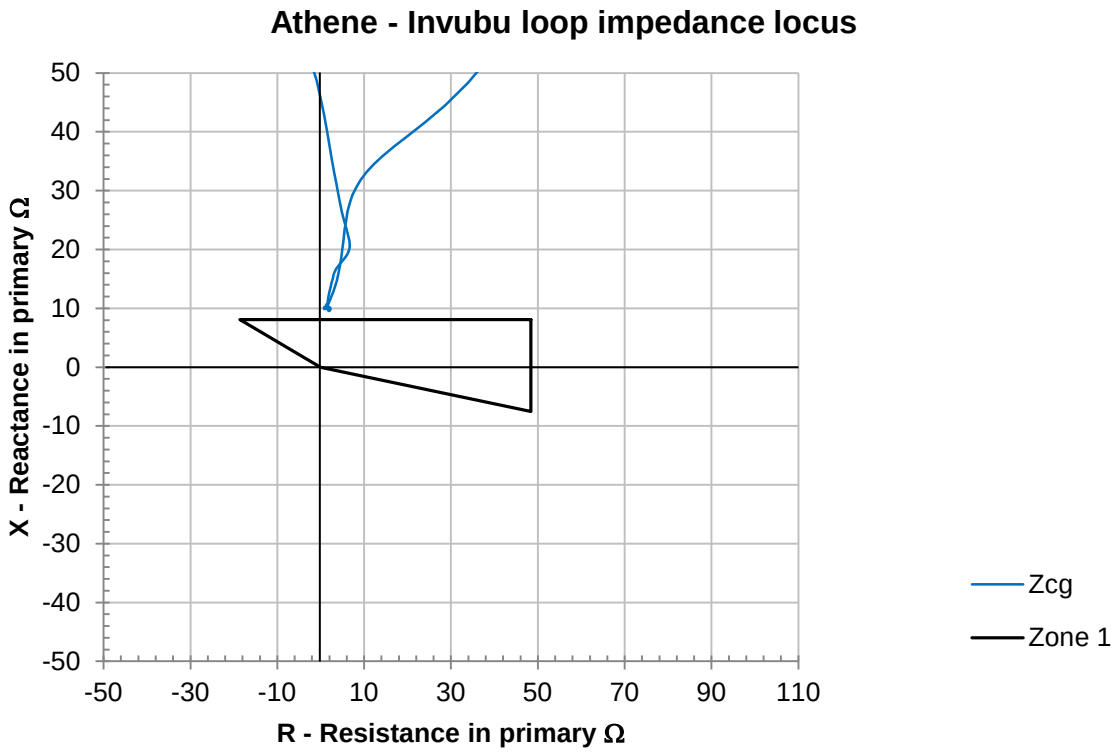

Figure 5.45: Athene - Invubu loop impedance relationship (after)

5.8.2 Hydra – Perseus 400 kV line

Section 5.3, covered the actual system incident, investigation and findings. The result of interaction between the system and MOV's that are responsible for sub-harmonic oscillations was highlighted in section 5.3.2, as well as the impact these oscillations had on the relay's measured impedance. The line impedance was measured and found to be within tolerable margins from the originally calculated values. The only shortcoming was the transient response compensation of the MOV's, which had not been implemented.

The protection settings were revised using the additional transient factor required for MOV-action as well as the already described R/X-ratio limitations. The reactive reach setting was reduced from 16.16 Ω to 12.75 Ω and implemented. Fault playback resulted in the relay at Hydra substation correctly not operating for the fault at Perseus substation. Of interest however is the fact that the impedance locus still passes through the relay characteristic. The time that the impedance locus remains within the relay characteristic was then determined from the fault data. It was found that this time duration was approximately 10.4 ms prior to any setting changes, whilst it reduced to 8.4 ms after reduction of the reactive reach by taking the transient factor associated with series compensation into account (Figure 5.46 and Figure 5.47 refers). With typical relay operation times of between 18 ms and 30 ms, as provided by the relay manufacturer in its performance guarantee, the question remained whether faults within the last 25% of the line, closer to the series capacitor bank, would yet again result in wrong relay operation [21].

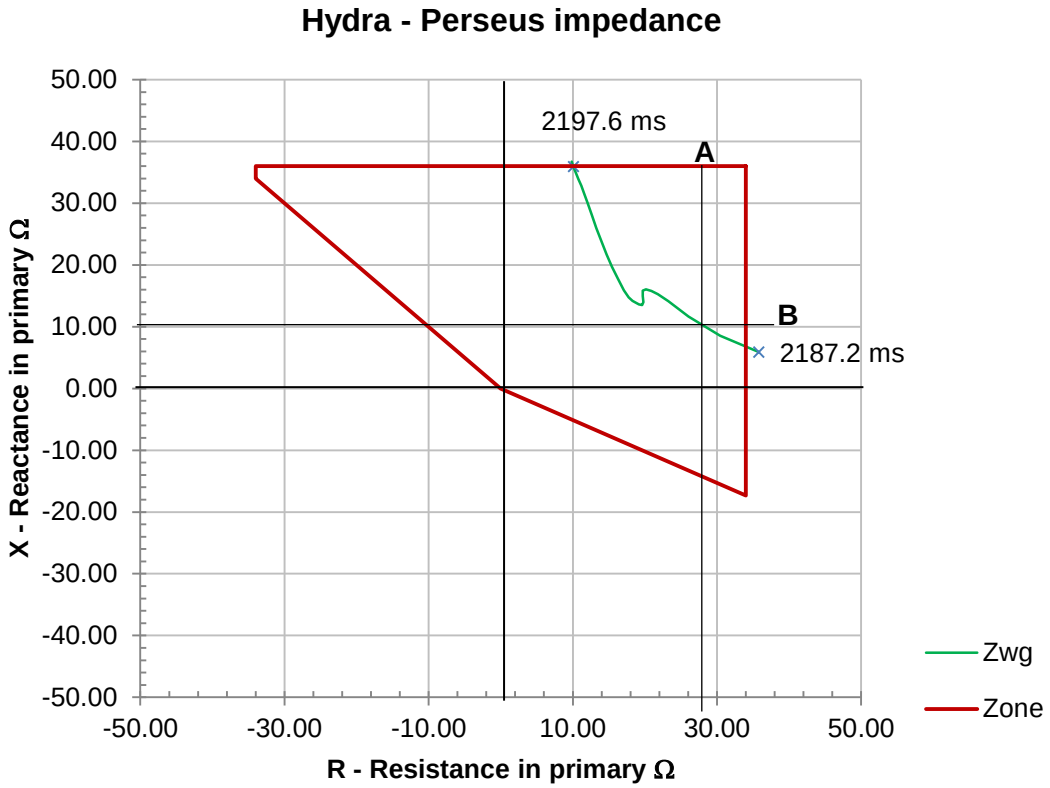

Figure 5.46: Hydra - Perseus impedance plot with time markers before change

This highlighted the impact that MOV's could have on impedance protection relays and triggered a revision of all relevant transmission circuit protection to include the transient sub-harmonic oscillation compensation factor. Figure 5.46 and Figure 5.47 also reflects the extent to which the impedance locus penetrates the zone 1 relay characteristic. A significant reduction in zone 1 reach indicated by lines (A) and (B) would be required for the impedance locus not to enter the zone 1 characteristic. A solution against relay maloperation would be to delay the zone 1 element with the time that the impedance locus remained within the zone 1 charateristic (+/- 9 ms in this case) after the reactive reach reduction required due to the sub-harmonic oscillations. Another approach would be to eliminate any possible mal-function of the zone 1 instantaneous element by disabling it. Permissive tripping, depending on tripping scheme selection are still available, effectively providing near instantaneous protection. The reliability of the carrier communication channels must however be evaluated, together with the impact to the system should it fail resulting in a long fault duration.

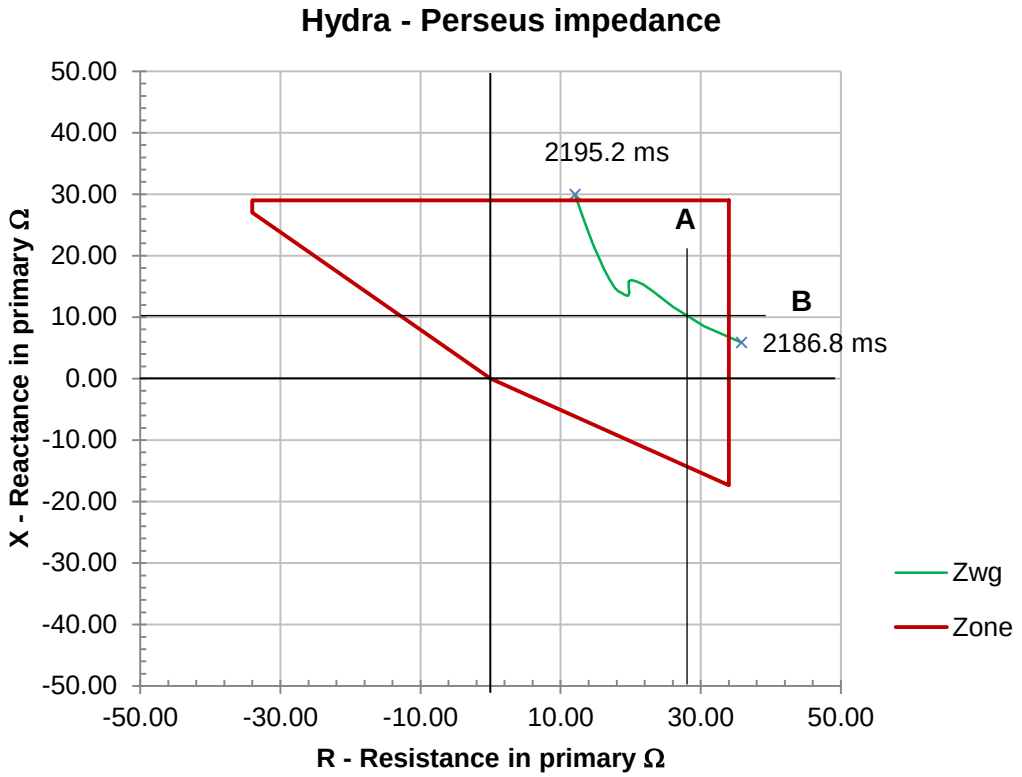

Figure 5.47: Hydra - Perseus impedance plot with time markers after change

It is therefore clear that the subharmonic oscillations that will be present during fault conditions causing the Metal Oxcide Varistors to conduct could be large enough to require switching off of the instantaneous distance protection zone 1. The decision to totally disable the zone 1 element should be carefully evaluated against carrier communication availability and the impact on the system in the event of carrier failure resulting in tripping times of greater or equal to 400 ms.

5.8.3 Georgedale – Klaarwater 275 kV line

This feeder, with a total length of 27.54 km, has a primary positive sequence $Z_1 = 1.041 + j8.7079\ \Omega$ and zero sequence impedance $Z0 = 9.907 + j30.86\ \Omega$ respectively. The following settings in primary quantities had originally been applied on the relay. ($R_{1e} = 27.89\ \Omega$, $X_1 = 6.95\ \Omega$).

In the loop domain the applied settings provided values for $X_1 = 12.86\ \Omega$ and $R_{1e} = 98.17\ \Omega$ primary ($K_r = 3.52$ and $K_x = 1.85$). With voltage and current transformation ratios of 2500/1 and 1600/1 respectively the actual secondary

resistive reach inclusive of the K_r-factor can be shown to be 62.83 Ω. This is significantly greater than the 20 Ω specified for overall transmission angles ≤ 60° discussed in section 5.4.

Table 5. 4: Summary of settings for Georgedale - Klaarwater feeder

Function	Reactance	Resistance - phase	Resistance - earth
Zone 1	X1 = 4.45 Ω	R1 = 17.85 Ω	R1e = 17.85 Ω
Zone 2	X1B = 7 Ω	R1B = 22.3 Ω	Comms. Controlled Zone
	X2 = 6.7 Ω	R2 = 20 Ω	R2e = 20 Ω
Zone 3	X3 = 6.7 Ω	R3 = 20 Ω	R3e = 20 Ω
Fault Detector	X+A = 10 Ω	RA1 = 20 Ω	RA1e = 20 Ω
	X-A = 5 Ω	RA2 = 20 Ω	RA2e = 20 Ω

The average transmission angle in the Eskom transmission system is approximately 30°, which is significantly smaller than 60° indicating that resistive settings larger than 20 Ω can be used. How much larger is however dependent on network dynamics, but the R/X-ratio of 6 as discussed in section 5.5.2 does provide a final limitation. The R/X-ratio, evaluated in loop domain, provided a value of 7.634 (98.17/12.86), which exceeds the allowable ratio of 6 by 27%.

Since the R/X-ratio is also applicable to the fault detection zone, the maximum resistive setting for this zone needs to be calculated first. The fault detector reverse reach (X-A) was set to 5 Ω secondary, giving an overall primary loop reactive impedance of 14.45 Ω ((5 * 1.85)/0.64). This in turn provides a fault detection maximum resistive reach (RA_2) of 86.72 Ω (55.5 Ω secondary), which equates to an actual setting on the relay of 55.5/3.52 = 15.77 Ω secondary ($RA_{2(sett)} = RA_{2loop}/K_r$). The different zone resistive reaches can now be set with some grading margin to that of the fault detector. Using a typical grading margin between zones of 20% to cater for relay and related primary equipment inaccuracies we obtain relay setting values for R3e, R1B and R1e of 12.62 Ω, 10.09 Ω and 8.07 Ω respectively.

These resistive relay settings will provide 69.41 Ω, 55.49 Ω and 44.39 Ω loop coverage, which in turn relates to actual primary fault resistive coverage of 59.46 Ω, 45.54 Ω and 34.44 Ω respectively after subtraction of the lines positive and zero sequence resistance values. With the average fault resistance distribution curve for Eskom, Transmission devision showing the majority of faults to be around 20 Ω, these new settings will provide adequate resistive coverage. These settings were evaluated utilising the same fault impedance locus, with the end result shown in Figure 5.48.

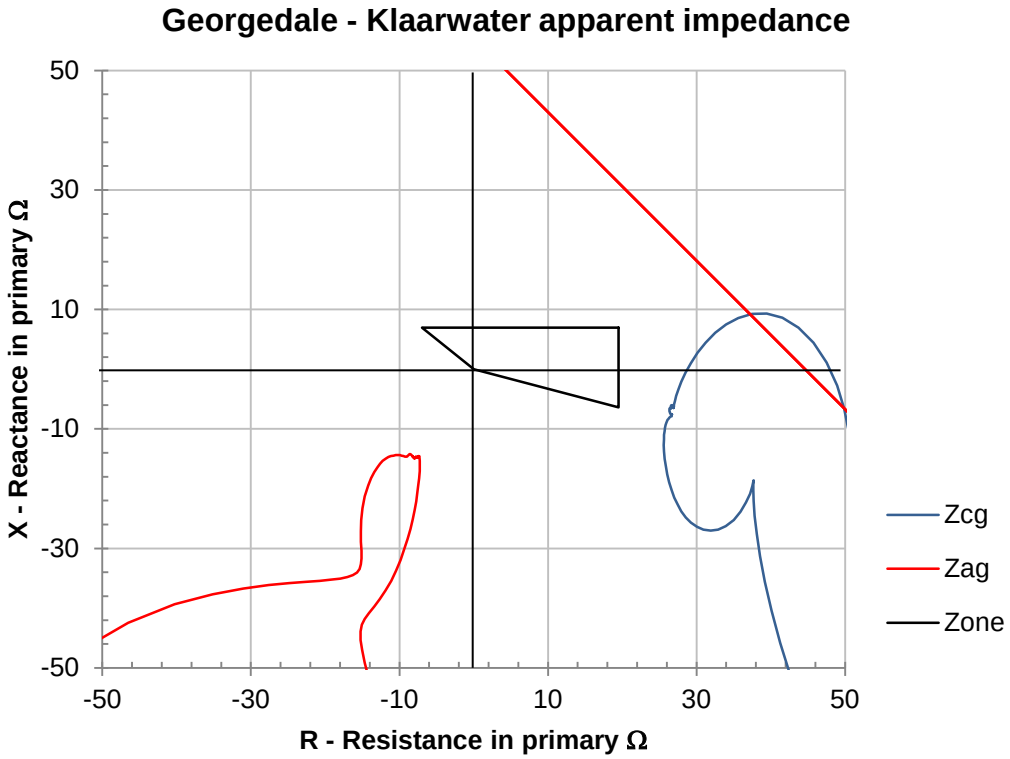

Figure 5.48: Revised settings with fault impedance locus

Secondary injection testing on the actual relay with the new settings implemented also confirmed that the relay was stable for the same fault condition. The values for the zone resistive reaches with the above method compares favourably with an R/X-ratio table provided for zone reach settings found in the Numerical Distance Protection by Gerhard Ziegler [6].

5.8.4 Etna – Taunus 275 kV line

This incident has been discussed in detail in section 5.5. The relay incorrectly tripped on the healthy C-phase current for a reverse A-phase-to-earth fault on an 88 kV feeder. It has been shown in section 5.5 that the R/X-ratio as set on the relay was greater than 9 when evaluated in the loop domain. This ratio exceeds the limitation of 6 as dictated by the manufacturer by a factor of 4.65 (27.91/6). The original relay settings in secondary Ω, were given as R_{1e} = 20 Ω, X_1 = 2.42 Ω, R_e/R_l = 5.11 and X_e/X_l = 1.19. With VTR = 275000/110 and CTR = 1600/1, this equates to primary ohmic values of R_{1e} = 31.25 Ω and X_1 = 3.78 Ω, with loop domain values calculated as R_{1e_Loop} = 190.94 Ω and X_{1_Loop} = 8.28 Ω. The relay settings were revised, bringing them in line with the performance guarantee for this length of line [21]. Values for R_{1e} and X_1 of 14.2 and 3.55 in primary Ω respectively were implemented. The result of superimposing the new apparent impedance relay characteristic with the actual fault locus is shown in Figure 5.49. Although the required result of the relay not operating for the healthy C-phase impedance locus, caused by the A-phase reverse fault, was achieved, the overall R/X-ratio in the loop domain was still exceeded. These relay settings provided an R/X-ratio in the loop domain of 11.15, still exceeding the value of 6, and provided a fault loop resistive coverage of 86.8 Ω.

It is considered an unnecessary risk to not set the relay within the advised R/X-ratio of 6, since another less resistive fault closer to the position of measurement could again result in wrong relay operation. It is proposed that a resistive setting of 4.1 Ω (6.41 Ω primary) should be used for the underreaching zone, resulting in an overall R/X-ratio of 5.04, whilst still providing a fault resistive coverage of approximately 39.2 Ω. Higher resistive coverage could be obtained with the time delayed overreaching zones, with the only limitation being the minimum load impedance. The final result is shown in the loop domain in Figure 5.50 illustrating that an effective fault resisitive coverage can still be achieved.

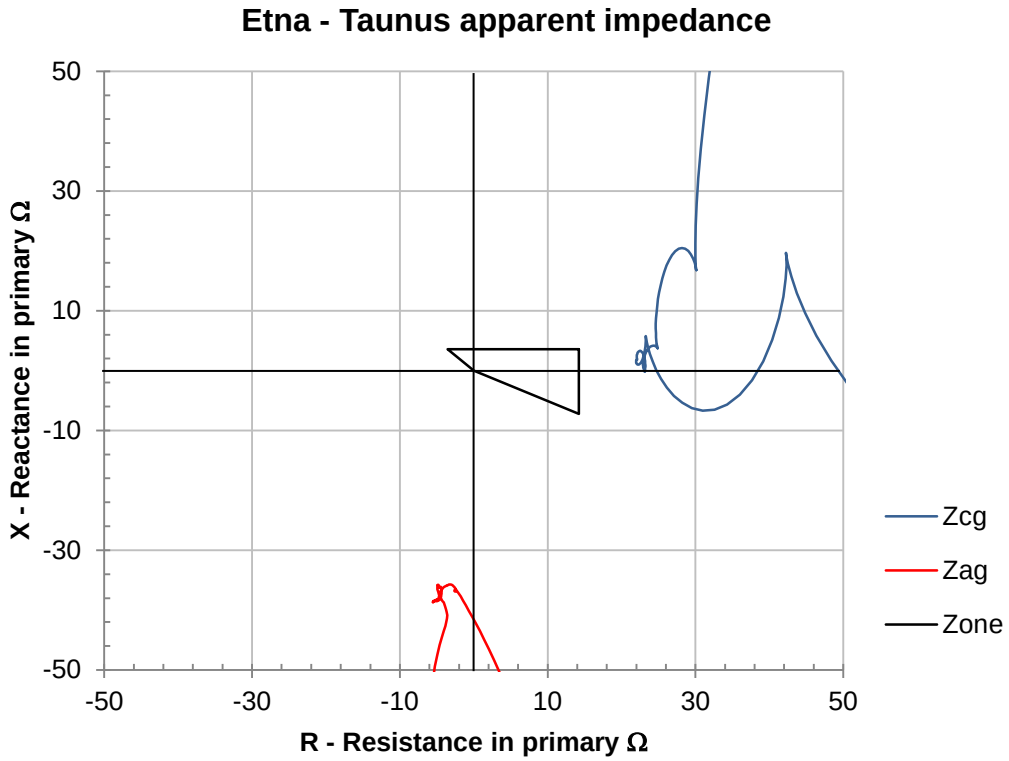

Figure 5.49: Atna - Taunus 275 kV fault impedance locus after changes

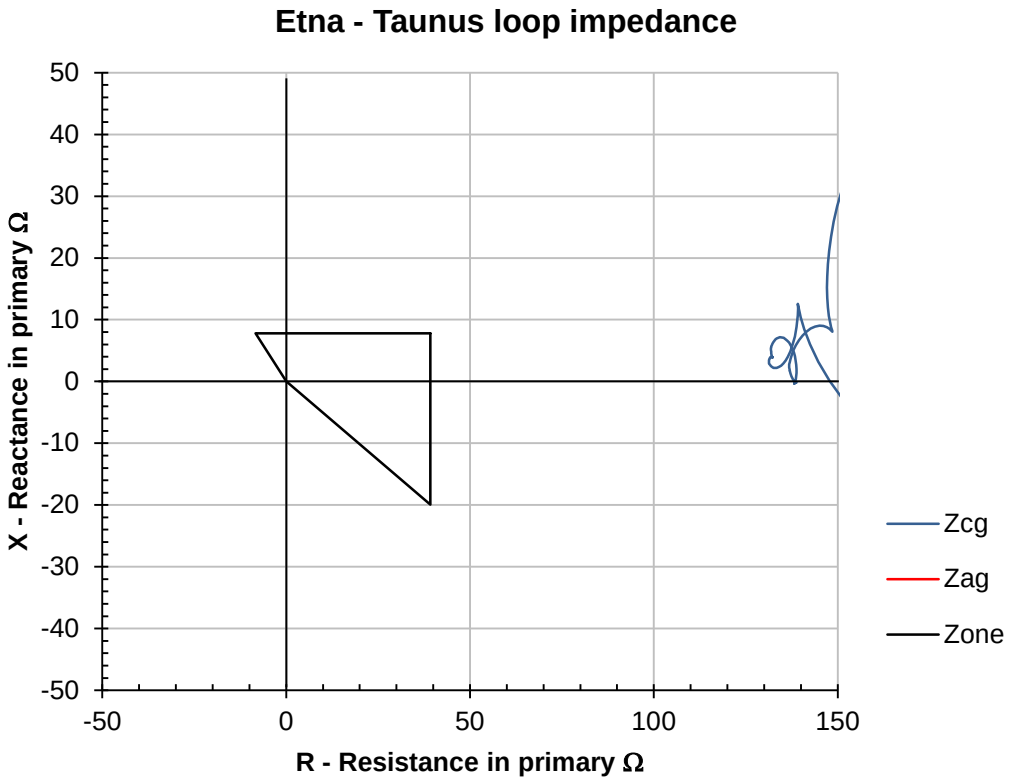

Figure 5.50: Etna - Taunus final impedance plot in loop domain

5.8.5 Bacchus – Droërivier 400 kV line

It was shown in section 5.6 that the phase selector settings of the relay had been inadequately set. It was also shown that correcting this would not entirely resolve the problem of not operating for the specific fault that occurred. The application of a high fault resistance detection comparison scheme, the reason for the high resistive fault and the associated slow fault development on the 400 kV system should be investigated. As a result of this study it is advised that the phase selector resistive reach $R_{FPE(phs)}$ be set to the value of 63.32 Ω, providing a primary loop resistive coverage of 143.9 Ω (63.32/0.44). The result is graphically represented in Figure 5.51.

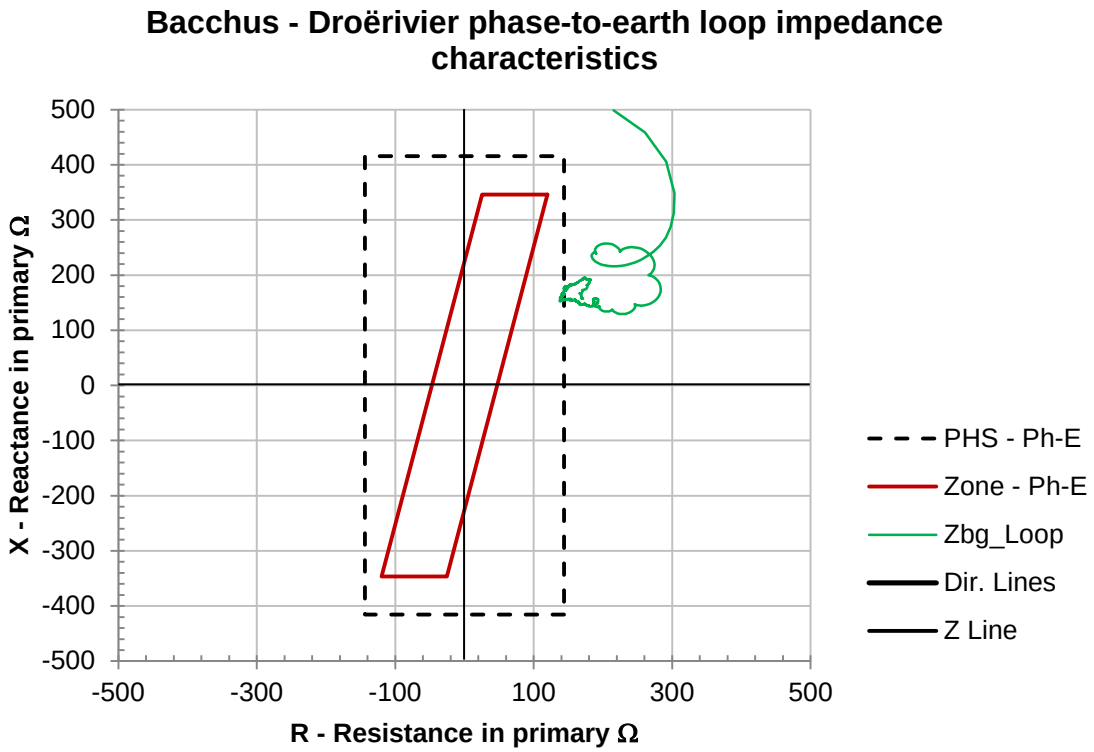

Figure 5.51: Bacchus - Droërivier impedance plot after phase-to-earth PHS setting correction

5.8.6 Leander - Grootvlei 400 kV line

Section 5.7 showed that the phase selector reach settings required optimization in the resistive plane. It is advised that the phase selectors resistive reach setting be changed to reflect an increase of approximately 1.9 pu ($R_{FPE(PHS)}$ = 69.3 Ω shown in the loop domain) above that of the permissive zone elements resistive reach setting ($R_{FPE(ZM2)}$ = 36.36 Ω), the result of which is shown in Figure 5.52 in primary quantities. The effect of the change is clear when the result shown in Figure 5.52 is compared with that shown in Figure 5.41, which reflects the relay characteristics prior to the setting change. The phase selector element would now be able to detect the fault well in advance of the impedance locus entering the zone element, ensuring proper phase selection and correct tripping.

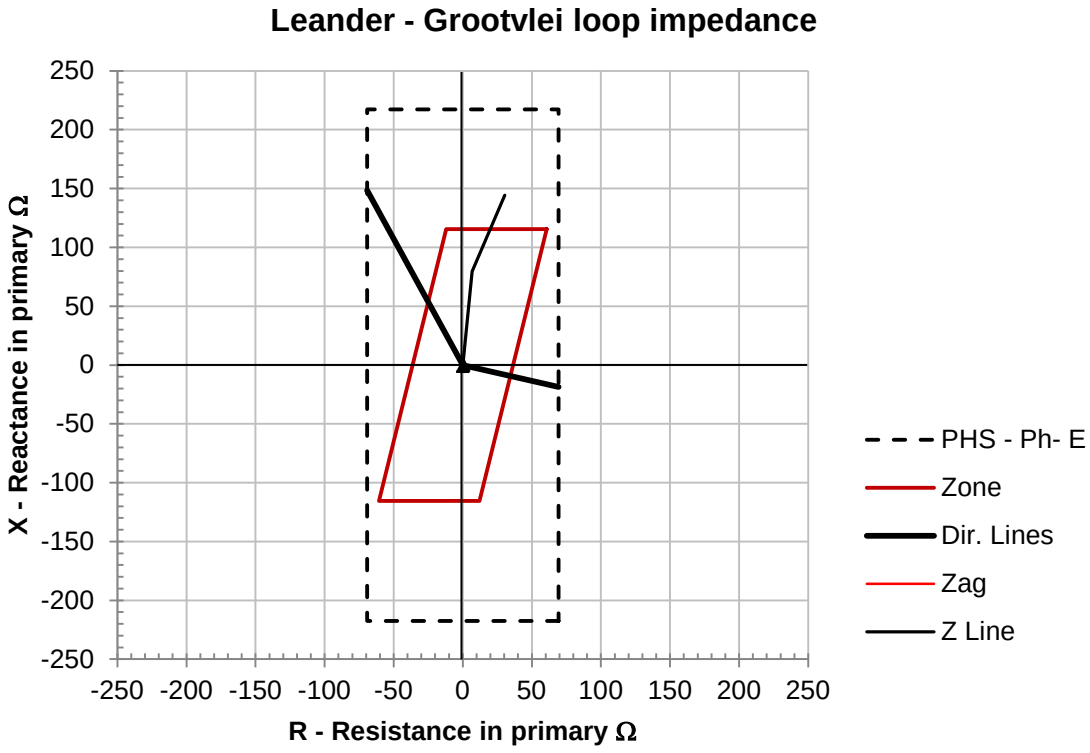

Figure 5.52: Leander - Grootvlei loop impedance, PHS reach corrected

Weak infeed was enabled on a later revision, and should remain so to allow operation of the relay under weak source conditions. The power swing detection settings have not been altered, since further investigation into the actual applied relay logic is required. This will however not be done as part of this research. It

must be stated that dynamic fault playback methods should be employed to verify the end result, after setting changes impacting on impedance measurements has been made, prior to final acceptance of the newly implemented relay settings.

Attempts are often made to compare the phase selector reaches that uses Ω/loop impedance settings with the zone elements that use a combination of Ω/phase and Ω/loop settings. The latter reach settings being for the zone reactive and resistive reaches respectively. The problem with this is that it provides a comparison of these elements on the same graph but in different domains (PHS in loop domain with the zone element in some combination of positive and loop). Great care has to be taken to ensure that plotting of fault impedance locusses is done using the different relay algorithms for the zone and phase selector elements. The correct relationship with respect to the impedance locusses can then only be obtained when the different locusses enter the respective relay characteristics at exactly the same time reference. The full impact of the above statement will be illustrated with the use of Figure 5.53. Focus will be given to the positive resistive side of the two impedance characteristics.

Phase Selector Earth (PHS-E) and Zone in Figure 5.53 reflects the relay characteristics associated with the original applied settings at the time of the fault using this combination domain approach. The two impedance locusses, based on the phase selector and zone algorithms, have been started at exactly the same instance in time of the fault recording with the zone impedance measurement locus Z_{ag} starting at the resistive edge of the zone characteristics. Figure 5.53 highlights the fact that the phase selector impedance measurement locus did not enter the set phase selector resistive reach at the same instant as is the case for the zone element. The phase selector resistive reach therefore has to be adjusted in order to achieve pickup at the same time as for the zone element, thus providing a higher resistive coverage for the phase selector element than was originally applied.

This new resistive value for the phase selector was established at 71 Ω primary (39.05 Ω secondary). It must be stated that this new phase selector resistive setting represents the absolute minimum value that must be set to achieve pickup of the

zone and phase selector elements at exactly the same time for the same fault. It must also be noted, as mentioned before, that it is a manufacturer's requirement to set the phase selector reach such that pickup for this element is established well before the fault locus reaches the zone elements in order to ensure correct phase selection and operation.

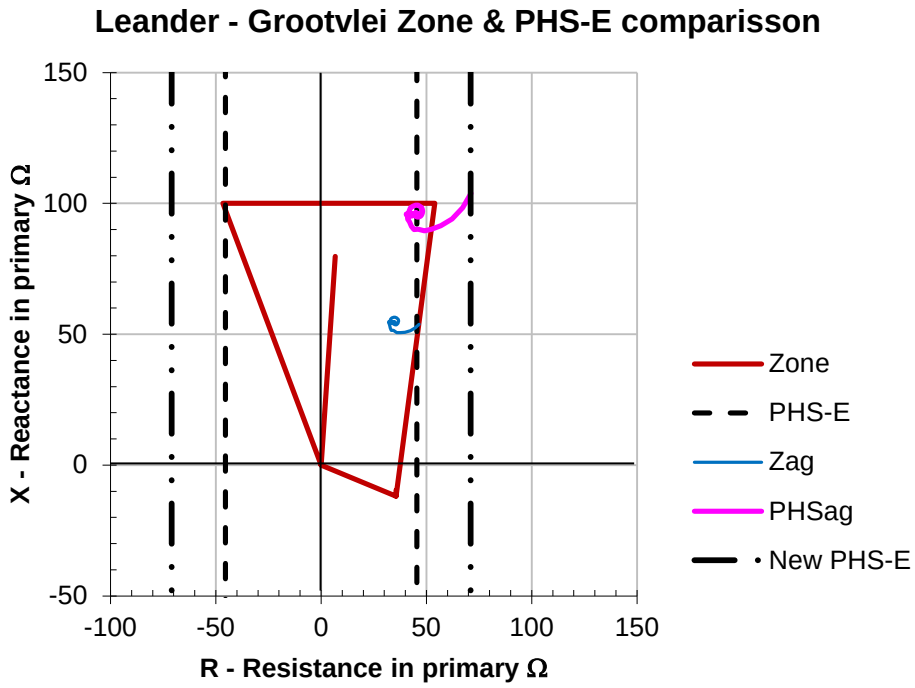

Figure 5.53: Leander - Grootvlei Zone and Phase Selector reach comparisson

Selecting a resistive reach setting of $R_{FPE(PHS)}$ = 1.2 * 71 = 85.2 Ω/loop on the phase selector will satisfy the required operational criteria. For this specific setting the new $R_{FPE(PHS)}$ setting closely resembles the applied phase-to-phase resistive setting $R_{FPP(PHS)}$ = 88.78 Ω/loop. Using the positive, negative and zero sequence theoretical circuits, it can be shown that in transmission systems where the load are normally connected in either delta or unearthed star, the load will play a desensitising role on the relay's reach ability due to the parallel path that is formed in the positive and negative sequence circuits. The amount of desensitising will be a factor of the fault position, the source and load impedance at the time of fault (see Figure 5.54 and Figure 5.55).

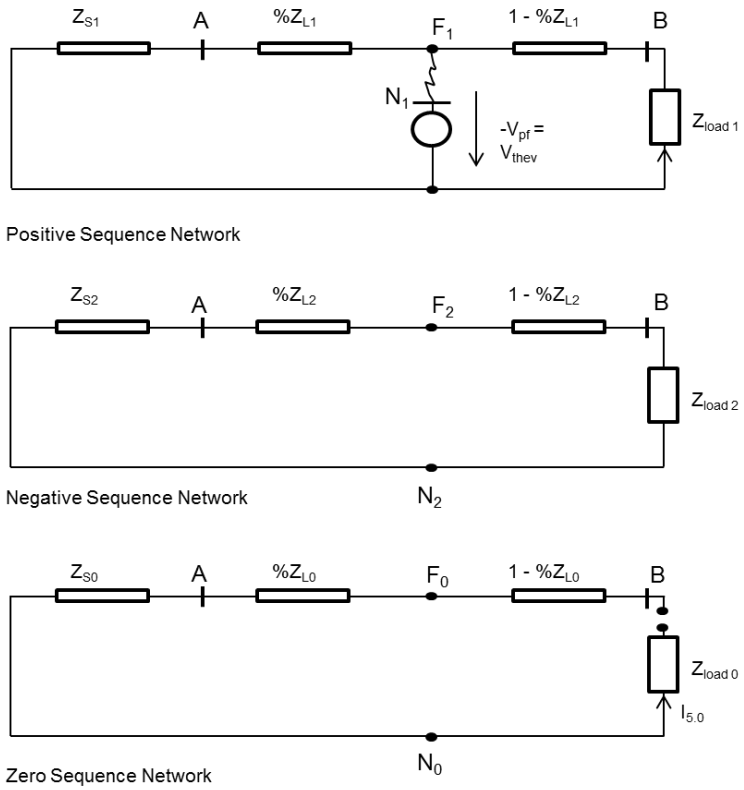

Figure 5.54: Sequence Network for a Phase-to-Earth fault in a radial network

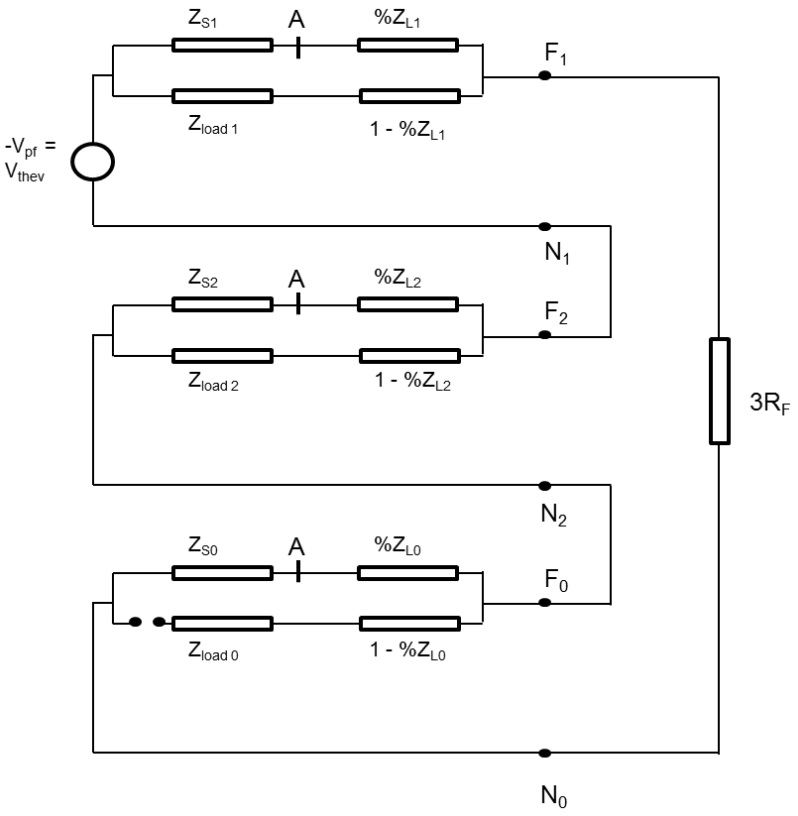

Figure 5.55: Simplified Sequence Network for Phase-to-Earth fault in radial network

5.9 Conclusions

Until now an effort was made to illustrate the complexity of the calculations, differences that exist and difficulties associated in the measurements of existing overhead conductor impedances, due to interferences from in-service circuits as well as some of the real risks involved with these measurements and the safety precautions that must be adhered to. The impact of representing a relay's measurements in the apparent impedance plane versus loop impedance plane and combinations thereof was illustrated, whilst the importance of relay fault detection and/or phase selection element pickup prior to the impedance locus entering the zone elements were also highlighted. The ease of misinterpreting results of measurements using the different algorithms for zone and phase selector when representing these characteristics in different domains on the same R/X-plane cannot be overstressed. New settings for the REL 531 relay's phase selector earth elements have been suggested for implementation. The decision to implement these changes resides with the management of protection relay settings within Eskom Transmission.

Representing the relay charateristics in the loop impedance plain is favoured since this provides the reader with a clear understanding and also provides the user with a proper comparison of relay reaches for co-ordination purposes. All impedance measurements, regardless of the actual relay algorithm, can be re-calculated into a loop quantity using the correct multiplications factors applicable to the specific impedance relay. The following chapters will endeavour to show the impact of load on the different relays.